Review

Wiley Online Library

ELECTROANALYSIS

doi.org/10.1002/elan.202100237

Electrochemical Nanobiosensors as Point-of-care Testing Solution to Cytokines Measurement Limitations

David J. Pérez,[a, b] Edwin B. Patiño,[b] and Jahir Orozco*[a]

Abstract: Most cytokines are present at reduced amounts in body fluids due to their biological features of production, release, and action mechanisms. The required time between sampling and their measurement is critical for diagnosis and treatment. Electrochemical nanobiosensors offer the possibility to be tailor-made and cost affordable, producing direct and rapid readouts with low sample volume, explaining their feasibility in timely measurements and potential in designing unique and multiplexed Point-Of-Care (POC) testing platforms. This review summarizes and discusses the measurement limitations of the standard methods and the recent progress on electrochemical nanobiosensors as a plausible alternative to measuring them.

Keywords: Cytokine · Biomarker · Electrochemical Nanobiosensor · Screen-Printed Electrode · Point-Of-Care Testing

1 Introduction

The primary response to any physiological insult done by a microorganism or another pathological condition relies on abrupt cytokines releasing [1]. The severe effects of the sudden and potent activity of massively released cytokines in the clinical context are critical complications that may drive a demise. The required time between sampling and their measurement is critical to apply any treatment. Point-of-care (POC) systems are medical assays done in place of patient care without needing a clinical lab infrastructure. Also known as the bedside, such devices provide prompt results, improving the diagnosis and treatment of secondary care. They may integrate electrochemical nanobiosensors to have an output signal in a concentration-dependent manner with high sensitivity and specificity. In this context, POC systems based on electrochemical nanobiosensors offer a potential solution to cytokines measurement limitations.

Cytokines are small glycoproteins (~6–70 kDa) that control immune response orchestration and cell communication. These macromolecules are soluble in body fluids as serum, plasma, urine, saliva, sweat, tears and others. Some of them modulate the most important nonspecific innate response, called inflammation, by both its induction (e.g., IL-1, IL-6, TNFα) or its blockade (e.g., IL-10, TGFβ). Other cytokines regulate the adaptative immune response either mediating the specification of immunity during antigen presentation (e.g., IL-2, IL-4, IL-12, IL-23) or as signature cytokines released by the different secretion profiles of T helper cells (e.g., Th1, Th2, Th17). Historically, cytokine classification has been too complicated because no systematic evolutionary criterium has been applied [2]. But classical textbooks dispose them into six categories: interleukin-1 (e.g., IL-1, IL-1Ra, IL-18, IL-33), hematopoietin (class I cytokines e.g., IL-2, IL-4, IL-5, IL-6, IL-13, IL-23), interferon (class II cytokines, e.g., IFN-α, IFN-β, IFNγ, IL-10), tumor necrosis factor (TNF, e.g., TNF-α, TNF-β), interleukin-17 (e.g., IL-17A, IL-17B) and chemokine families (e.g., IL-8, CXCL2, CCL2, CCL5). Homeostatic cytokines are produced all the time, having basal levels in their soluble form even whether there is no stimulus; meanwhile, those that potentiate or inhibit the inflammatory response are called pro- or anti-inflammatory cytokines, respectively. Most attempts to develop POC systems based on electrochemical nanobiosensors have been for pro-inflammatory cytokines, given their role as diagnostic and prognostic biomarkers. In principle, they may be used as devices to follow a chronic condition such as the glucose biosensor for diabetic patients.

The commercial methodologies applied in cytokines testing remain not harmonized but are also intrinsically limited by cytokines' physiology (see below). Recent advances of electrochemical nanobiosensors in POC-testing formats put them in a promising place as possible solutions to those physiological limitations [3]. Two recently published reviews discussed several electrochemical biosensors' elements for assessing pro-inflammatory cytokine levels during the cytokine storm produced by SARS-CoV-2 or other non-infectious diseases, such as neurodegeneration and cancer [4,5]. Yet, in this review, we discuss how the hindrance imposed by the biology of cytokines behavior, together with technical and methodological limitations for their analysis, may be overcome by

[a] D. J. Pérez, J. Orozco
Max Planck Tandem Group in Nanobioengineering, University of Antioquia, Complejo Ruta N, Calle 67, N° 52–20, 050010 Medellín, Colombia
E-mail: grupotandem.nanobioe@udea.edu.co
[b] D. J. Pérez, E. B. Patiño
Grupo de Bioquímica Estructural de Macromoléculas, Chemistry Institute, University of Antioquia, Lab 1–314, Calle 67, N° 53–108, 050010 Medellín, Colombia

developing electrochemical nanobiosensor-based POC systems, emphasizing in the screen-printed electrode (SPE) platforms, but detailing some distinct electrochemical formats. Additionally, some preanalytical considerations are presented to stimulate the discussion about the urgent requirements for harmonized cytokine measurement and the opportunities that offer POC testing in the context of ASSURED criteria (i.e., Affordable, Sensitive, Specific, User-friendly, Rapid and robust, Equipment-free and Deliverable to end-users).

1.1 Physiology of Cytokines Behavior: A Biological Limitation for their Measurement

Despite the stage, any cytokine must reach its cognate receptor to complete the associated biological function. To do that, cytokines "exploit" almost all cell communication strategies. However, the pivotal issue about their physiological behavior as communication mediators is related to the fact that their effects tend to be restricted to a given microenvironment, acting as intra-, yuxta-, auto- and paracrine factors compared with its endocrine effects (Figure 1). The advantages, challenges and technical implications for cytokines measurement may be deduced from brief examples. Counterintuitively, some cytokines as alarmins (e.g., IL-1α, IL-33, HMGB1) are maintained intracellularly to accomplish essential functions once they are produced (intracrine in Figure 1). For instance, IL-33 is retro-transported and cumulated into the nucleus [6], where it mediates the chromatin compaction by the promotion of the nucleosome-nucleosome interactions [7] and the transcription modulation [6,8,9], a skill that remains unconfirmed [10]. After an exogenous insult, IL-33 alarmin is released to extracellular space and complexed with histones, which confers it a tunable effect, controlling the free IL-33 availability after necrosis or synergizing (i.e., additive effects) to initiate its pro-inflammatory effect [11,12]. In summary, some cytokines' basal distribution, like IL-33, suggests an intracellular role, functioning as intracrine factors, while they are not generally present in any body fluid.

Similarly, some cytokines mediate physiological processes in a juxtacrine manner, in which either the ligand or the receptor must be held to the membrane of two adjoined interacting cells, instead, be released (Figure 1). A notable example is the tumor necrosis factor (TNF), a pleiotropic cytokine (i.e., acts over more than one cell target) that can exert a myriad of roles, according to the context and held receptors (i.e., TNFR1 and TNFR2). TNF may exist held to membrane (mTNF, 26 kDa) [13,14], or can be actively cleaved to a plasma soluble form (sTNF, 17 kDa) [13]. The mTNF tends to be expressed by the monocyte/macrophage system and lymphocytes, interacting primarily with TNFR2 and

David J. Pérez received his B.S. degree in microbiology from the University of Antioquia (UdeA), Colombia. Then, he finished his master degree in the Corporación de Ciencias Básicas Biomédicas (CCBB) at the Faculty of Medicine from the same university. In 2020, with the support of a research fellowship from MinCiencias (Colombia), he started PhD studies in electrochemical biosensors for interleukins monitoring under the supervision of Professors Jahir Orozco and Edwin Patiño. His research interests include surface functionalization of electrodes with nanoparticles and synthesis, extraction and purification of engineered proteins for further functionalization of nanostructured transducers for cytokines detection in corporal fluids.

Edwin B. Patiño is a biochemistry professor at the Faculty of Chemistry, (UdeA, Colombia). He is the current director of Bioquímica Estructural de Macromoléculas research group, from the same university. He obtained his B.S degree in biology from UdeA, and finished his master degree at the CCBB (Faculty of Medicine, UdeA). Then he went to Julius Maximilians Universität Würzburg (Germany) where received his PhD degree in physiological chemistry (2002–2008). His research work is focused on genetic engineering for massive recombinant protein production with useful tags.

Jahir Orozco is a chemist from the UdeA (Colombia), with a Ph.D. in chemistry from the University of Barcelona and the Institute for Microelectronics of Barcelona (Spain, 2008). He completed three postdoctoral stays for sevent years at the Banyuls sur Mer Oceanological Observatory (France), the Department of Nanoengineering at UCSD (USA) and the Catalan Institute for Nanoscience and Nanotechnology (Spain). He is currently the group leader of the Max Planck Tandem Group in Nanobioengineering (MPTG-N, UdeA) and an editorial board member of the Molecules journal. His areas of interest include nano(bio)technology, nano(micro)carriers, nanomotors, nano (micro)devices, nanomaterials, (bio)sensors, electrochemistry, and development of analytical tools for environmental and biomedical applications.

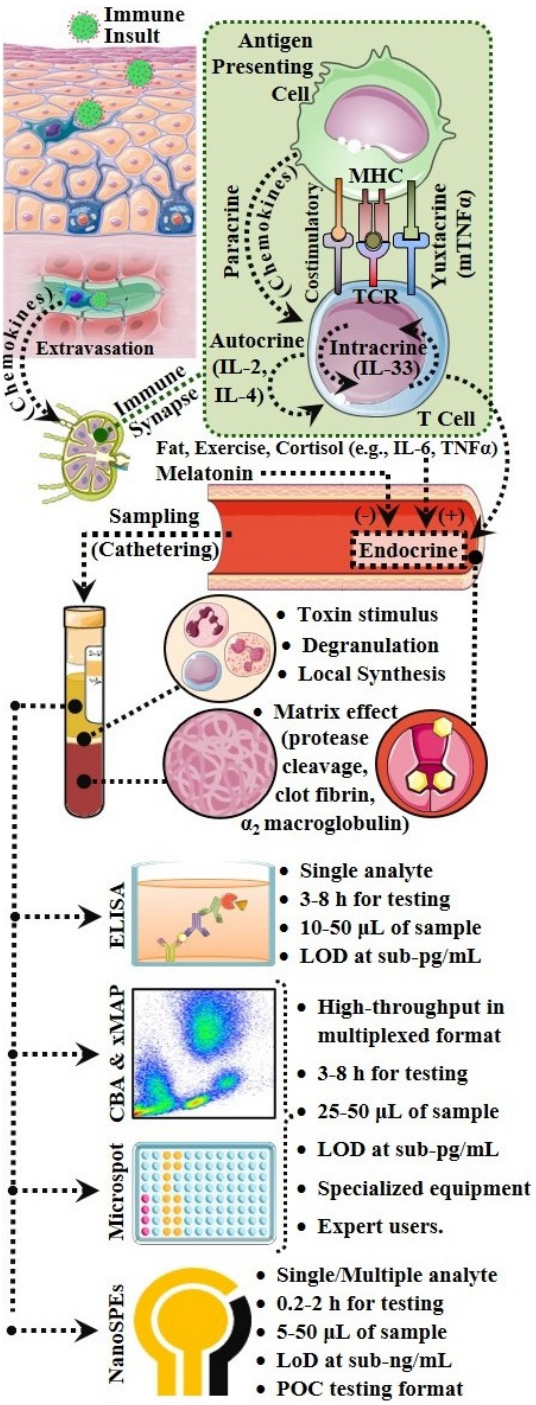

Fig. 1. Physiological cytokines behavior determines their levels at any corporal fluid, with an especial emphasis on blood. After sampling, it may be processed by conventional tests (e.g., ELISA, flow cytometry-based methods, Microspot) or by the use of electrochemical techniques. Some features are highlighted on the right side. In parentheses, examples do not exactly represent the drawn situation. See the text for more details. Some images were taken from free smart servier medical art.

mediating processes as lymphocyte proliferation and activation [15,16]. On the other hand, sTNF acts mainly by the union to TNFR1 and mediates either pro-inflammatory or cell death-related effects (e.g., apoptosis or necroptosis) [17]. Hence, the observation that cytokines' physiological flexibility includes the juxtacrine form of communication highlights that some functional forms, as held to the membrane, cannot be measured at a clinical laboratory with the available technology, unlike electrochemical techniques coupled to microfluidic systems (see below).

Assuming a random antigen searching of immune cells into a confined space (e.g., lymph node) or a liquid or semiliquid diffusion medium, the extracellular cytokine concentration is approximately proportional to the inverse of the square of the distance from the releasing cell [18]. Consequently, the cytokine spread rate depends on released cytokine production and consumption competing processes [19]. This fact modulates the immune response by both cell orientation during migration and gene expression induction (e.g., polarization). The extracellular matrix adsorption and swarming must also be considered because they force a short action radius of cytokines activity. For instance, once a potential immunogen is phagocytosed at a given tissue (e.g., skin), the antigen-presenting cell (APC) inclines to use the lymph as the flow medium to migrate. This liquid circulates into lymph vessels until it reaches its nodes. The spatial disposition of lymph increases the probability of encounter two leukocytes to form an immune synapsis (IS) (e.g., between classical dendritic cells (cDC) and T cells (LT) (Figure 1). In essence, the actively secreted chemokines serve either as a stimulus to extravasate (e.g., CC-chemokine ligand 19, CCL19 and CCL-21), when passing tangentially to cells of high endothelial venules (HEVs) or during intranodal cell migration (e.g., of CCL21, CXCL13) [20,21].

It is probable that the biological sense that explains cytokines' close action radius, be a quantitative threshold, so that a massive focused secretion of a specific type of cytokines polarize the signaling of the target cell towards a precise effect but, at the same time, the other simultaneous signals from surrounding microenvironment are lessened or ignored [19]. As a way of illustration, it has been proposed that the strong activation of macrophages by the union of high-avidity ligands (e.g., immune complexes) to the immunoreceptor tyrosine-based activation motif (ITAM)-coupled receptors induces transient calcium signals that block the cytokine receptors and synergies with Toll-like receptors (TLR) signaling. In contrast, the low-avidity ligands (e.g., monomeric IgG) of ITAM-coupled receptors cause the inverse effect [22]. Another benchmark case occurs in T lymphocyte activation during IS. Here, the T cell receptor (TCR) holds to a peptide charged major histocompatibility complex (pMHC), on the surface of an APC and, at the same time, costimulatory receptors (e.g., CD40-CD40L, CD80/CD86-CD28) must come together yuxtacrinally (Figure 1). The pair TCR-pMHC and costimulatory complexes are surrounded and sealed by other molecules allowing a cytokine-directed secretion to T cells into the

IS, in a paracrine manner that acts as the third required signal to promote its proper activation and polarization during antigen presentation [23,24,25]. In the end, some cytokines do not spread significantly beyond the two interacting cells (e.g., IL-2 and IFNγ), while others are multi-directionally secreted (e.g., TNF, CCL3) [26]. Furthermore, evidence suggests a controlled releasing process by exo- and ectosomes during IS exchange [27]. Thus, it is important to investigate if the cytokines can also be included in vesicles but did not freely release [28], decreasing their body fluids levels.

After $CD4^+$ T cells polarize into helper specialized phenotypes (e.g., Th1, Th2, Th9, Th17), they are inclined to release a close group of cytokines. A tangible case is a Th2 profile. The IL-4 sign from primed T cell itself (i.e., autocrine) and surrounding cells, together with the activation signals provided by dendritic cells (e.g., IL-25, IL-33), synergizes in a paracrine manner [29], leading to the polarization of the Th2 cell, while Th1 and Th17 cell responses are suppressed [30]. Once differentiated, Th2 synthesizes its signature cytokines (i.e., IL-4, IL-5 and IL-13). The IL-4, together with IL-13, induces the class switching to IgE and IgG1 over B lymphocytes [31] and promotes the alternative activation of macrophages [32,33]. For its part, the wrench-like form by which the IL-5 receptor alpha chain (IL-5Rα) binds its ligand (i.e., IL-5) seems to trigger conformational changes that initiate the signaling activity of typical β chain (IL-5Rβ_c), up-regulating the eosinophil metabolism and its effector mechanisms (e.g., degranulation) [34,35].

The cytokine release also occurs in a nonspecific manner when it is induced by activation of innate mechanisms (e.g., TLR signaling). In this scenario, both immune and non-immune cells can serve as a source. In the beginning, these cells′ cytokine discharge acts in an autocrine and paracrine way. But, when the immune system is significantly challenged, several cytokines, but especially the endogenous pyrogens (e.g., IL-1, IL-6, TNFα), can act far away from being released in an endocrine form.

These synergistic molecules may travel, even at a sub-nanomolar concentration, until hypothalamic thermal regulator centers, resulting in vasoconstriction, shivering and brown adipose tissue activation, which in turn leads to a systemic thermal increase (i.e., fever) [36,37]. In the classical endocrine pathway, the IL-6 circulates until it reaches the liver, inducing the hepatic production of positive acute-phase proteins (e.g., c reactive protein, CRP; serum amyloid A protein, SAA), but alternatively, it may act held to its soluble receptor (sIL-6R), leading to systemic pro-inflammatory effects [38,39,40,41,42]. Finally, there is evidence that TNF pyrogen also has notable systemic effects, especially on the cardiovascular (e.g., bradycardia) and muscle systems (e.g., myocyte apoptosis) [43].

Notice that the initial source may be the local tissular cells like macrophages, but during severe diseases, when cytokines serum levels are important, the endocrine effect synergies with the local autocrine release [44]. Because of their physiological role, it may be expected that the cytokines with an endocrine behavior, like pyrogens, have basal monitorable levels at a steady state and that their systemic noxious effects could be valued as a function of their serum concentration increase in extreme situations (e.g., systemic inflammation). This feature differentiates these cytokines from hormones, being incomparably more active than the latter because they act at sub-pM levels [45]. Besides, some of the endocrine cytokines undergo a neuroendocrine control showing greater levels in the morning (e.g., IL-1, IL-6, TNF-α, IFNγ), which correlates inversely with nocturnal melatonin rhythm [46] but proportionally to awake cortisol peak (Figure 1) [47]. Cytokines also may fluctuate according to the lifestyle affecting, in turn, the circadian clock rhythm by the induction/repression of clock proteins [48,49]. For example, it has been proposed that TNF-α and IL-6 may serve as mediators by which fat diet (i.e., high fat and saturated fatty acids diet) induces inflammation, feeds back and modulates fundamental circadian properties of peripheral clocks [50]. There is also evidence that IL-6 is produced by the muscle throughout exercise, acting in an endocrine manner over the liver to induce hepatic glucose output and lipolysis [51,52]. Finally, there is evidence that a fraction of circulating cytokines is held to α2-macroglobulin carrier protein and undergoes degradation by extracellular proteases (Figure 1), which decrease its availability to be tested, masking its actual levels [53,54].

After physiological troubleshooting associated with immune challenges, the cytokine production is shut down, reaching homeostasis again. The above implies that cytokine measurement is useful when they accumulate, surpassing the threshold to be significatively functional or pathological (i.e., when cytokine levels > effective concentration for the half-maximum response, EC50). Hence, in principle, it is possible to correlate a cytokine production fingerprint to different phases and types of disease progression during treatment [55,56,57]. Nonetheless, it is important to consider that most of them have extremely low basal levels, or even they have not, meanwhile cytokines with endocrine roles (pyrogens mainly) have baseline ranges that oscillate as a consequence of multiple stimuli (e.g., stress, diet, exercise). In the first situation, detectable serum or plasma levels are not necessarily associated with an endocrine function but instead to a basal leakage or a surpass from its local action threshold, serving as disease severity biomarkers. Similarly, when pyrogenic cytokines reach high serum levels, a hyperinflammatory harmful state is installed in the host, called a cytokine storm. Three criteria have been proposed to determine the later state: (i) acute systemic inflammatory signs (i.e., fever, fatigue, anorexia, headache, rash, diarrhea, arthralgia, myalgia, and neuropsychiatric findings), (ii) secondary organ dysfunction (e.g., renal, hepatic, or pulmonary), and (iii) elevated circulating cytokine levels [58]. Furthermore, since their pleiotropy, most cytokines are not ideal biomarkers alone

because an individual cytokine level in patients cannot specify a unique disease (or prognosis) in comparison with levels in a control group of healthy subjects or treated patients [21,59,60]. The most reasonable way to include these molecules as biomarkers in situations like cytokines storm is their simultaneous multiple detections (i.e., multiplexing).

1.2 Technical Limitations of (Pre)Analytical Procedures to Cytokines Measurement

Overall, there are no standardized baseline levels for cytokines, which may be associated with technical issues as the absence of harmonized preanalytical and analytical protocols [61]. An important observation is related to the method used for sampling. At least, three important phenomena may increase the cytokines level after sampling (Figure 1), namely, (i) their synthesis induced by the material of the sampling tube (e.g., polyvinyl chloride induces a marginal increase of IL-1β, IL-6, IL-10 and TNF-α, but markedly IL-8 and MCP-1) [62], (ii) a degranulation process during clotting and the further cytokine release to the serum [63], (iii) the presence of pyrogenic endotoxins in sampling tubes that stimulates a synthesis *de novo* (e.g., IL-1β, IL-6, TNF-α) [64]. It has been demonstrated that indwelling venous catheters also stimulate the local cytokine production (e.g., IL-6), leading to a misinterpretation of the actual systemic levels in the patient [65,66]. In contrast, both the proteases mediated degradation, after two hours of storage, as well as the matrix adsorption (e.g., fibrin, α2-macroglobulin, albumin, anti-cytokine antibodies) can explain the decrease in serum respect plasma partially [67,68]. Some studies have shown that the (defibrinated) plasma levels do not correlate with serum cytokine levels. Even if the plasma samples are obtained with different anticoagulants (e.g., ACD, heparin, EDTA), the cytokine levels vary significantly independently if unique or multiplexed kits are used [59,62,63,64,67,69,70]. Remarkably, measured cytokine secretion profiles were nearer between ethylenediaminetetraacetic acid (EDTA) and acid-citrate-dextrose (ADC) used as an anticoagulant [59].

Along with the challenges associated with the cytokines' physiological behavior, the commented technical limitations can partially explain the enormous interindividual variability reported elsewhere [63,71]. In this line, several cytokine levels may increase (e.g., IL-1β, IL-7, IL-12p70) or get down (e.g., Flt-3 Ligand) between age groups [59]. Similarly, although they did not report differences associable to sex, independently of sample conditions, other studies have shown both increases (e.g., CCL9, XCL1, CXCL11) and decreases (e.g., CXCL10, CXCL12, CXCL16) during ovulation, which may be interpreted as a prelude of uterus NK cell homing [72].

1.3 Common Technology Used to Measure Cytokine in Clinically Relevant Conditions

The plethora of techniques oriented to measure cytokines massively has been reviewed [60,73]. Outstandingly, the later papers coincide with the potential of ultrasensitive nanobiosensors (i.e., fM, aM) and call about their issues to analyze complex matrices (e.g., nonspecific binding (NSB) and fouling). Despite plenty of available ways to measure cytokines, testing them generally relies on antibody-based capture immunoassays. Enzyme-linked immunosorbent assay (ELISA) is the gold standard method for clinical protein measurements [74]. The most critical limitation of ELISA is that it just detects one analyte per kit. Additionally, ELISA is expensive, requires extensive analysis time (3–8 h), needs a relatively large sample size (10–100 μL), has a near dynamic range and is difficult to adapt to POC use. As mentioned above, the immune response is governed by tens of cytokines, so multiplexing formats are highly desirable. Several cytokines are simultaneously tested in a single assay using a single sample [71,[75]. The most used multiplexed way to measure cytokines is the cytometric bead array (CBA) and Luminex xMAP technology (x = analyte, Multi-Analyte Profiling) [76,77,78]. Polystyrene magnetic microbeads (~6 μm) are stained with internal dyes with variable intensities, being possible to discriminate them by the fluorescence (FL2) and size (FL3) parameters. CBA assays enable measuring ~30 proteins simultaneously, while xMAP can discriminate until 100 types of different analytes because it uses different ratios of red and near-infrared fluorophores, increasing its multiplexing degree [75,76]. Nevertheless, while CBA requires any flow cytometer, Luminex uses a particular machine for its specific purpose [77]. Both technologies use a specific protein-capturing antibody conjugated onto the bead surface. A secondary antibody with a specific fluorescence intensity is used for analyte detection [78]. The required volumes oscillate between 25 to 50 μL of serum for all analytes, compared with 50 to 200 μL of serum per analyte needed for a conventional ELISA. Luminex-based kits are not optimal at sub-pg/mL concentrations but may have a greater dynamic range (1–1000 pg/mL) than ELISA [63,71]. Some examples illustrate the usefulness and limitations of these multiplexed technologies in diverse clinical situations.

For example, Drop assay (DA) on beads in conjunction with multiplexed Luminex technology has been done with small volumes of tears (5 μL) to improve the ocular disease diagnosis. In a similar study, the levels of the proinflammatory cytokine were measured with a very low limit of detection (LOD ~1 pg/mL) and spread detection ranges (e.g., IL-1β, 2.41–2502 pg/mL; IL-6, 2.47–2497 pg/mL; TNF-α, 4.98–16024 pg/mL; IFNγ 10.06–37464 pg/mL) [79]. Interestingly, in this study, just IL-1β was not detected in all of the 1000 healthy participants, suggesting very low or not basal levels of it in tears, which correlates with other studies on the serum from healthy individuals

[80,81] but contrasts with some exposure to industrial pollutants [82]. For instance, a study that used four types of tests, two based in Luminex 100 system and two based in CBA, indicated that IL-1β was detected in almost all supernatants of isolated white cell cultures from healthy Spain and Mozambique participants (endemic for malaria), that were exposed to *Plasmodium falciparum* antigens [83]. This observation agrees with the proposed early role in immunity response for IL-1β and suggests that its levels in the blood can be correlated with disease severity [84], but raises the question about if the sensitivity of used techniques was sufficient to detect it. Bacterial infection severity also has been correlated with IL-1β and other pro-inflammatory cytokines (i.e., IL-6, IL-7, IL-8, IL-10, IL-13, TNF-α, IFN-α, MCP-1). It suggests that their levels significantly increased in septic shock in comparison with severe sepsis when they were measured with a 17-multiplexed kit (Bio-Rad), which in turn showed a good correlation with ELISA measurements ($r = 0.815$; $P < 0.001$) [85].

There are also approaches to characterize the blood-related chronic course diseases as a cytokine level's function [57]. For instance, by the use of a 12-plexed assay, a study showed that it was possible to discriminate the similar symptoms of patients with secondary polycythemia (SP) and polycythemia vera (PV) from the fact that SP patients showed decreased plasma levels of the IL-17A, IFNγ, IL-12p70 and TNF-α oncoinflammatory factors, in comparison to PV patients [86]. In contrast, a 25-plexed bead array done with blister fluids from patients with complex regional pain syndrome type 1 failed to detect several cytokines (e.g., IL-1β, IL-2, IL-5, IL-7, IL-15, IFNγ) that were detected by more sensitive ELISA kits [87].

Immulite® is another commercial bead multiplexed technology for the determination of cytokine levels that is relied on chemiluminescence. It has shown high run precision, short incubation times and calibration stability (e.g., two weeks), but it needs relatively high volumes (e.g., 350 μL), which should be no ideal, manly for pediatric samples [88].

The microspot array is another method based on printing many spots at 96-well plates of different materials (e.g., polylysine and aminopropyl silane, epoxy silane-treated glass, polyvinylidene difluoride and nitrocellulose- or nylon-based membranes) [75,[89]. This technology enables relatively easy in-house tailoring, being proven its multiple cytokine measurement reliability in fluids such as plasma, serum, urine, conditioned medium, tissue and cell culture lysates [90,91,92,93]. Besides, microspoting maintains ELISA specificity, has a high throughput, and permits the same antibody label versatility (e.g., chemiluminescence, fluorescence). In contrast, it requires high volumes and processing time, compared with bead-based methodologies and shows variations as ~10 % when are made at home [92]. For instance, a microstpot-based platform showed an 810-multiplexing degree but did require 200 μL of the sample, >3 h to be processed, and its coefficient of variation (CV) did oscillate between 5–15 % [94].

2 Electrochemical Nanobiosensors and its Potential Advantages in Cytokines Determination

Most multiplexed commercial tests for cytokine determinations are based on beads and multi-well plates, as those commented before, and have been used for massive studies (e.g., clinical trials, epidemiologic studies) [59,63,69,81,83]. Nevertheless, nanobiosensors can be easily used in a unique or multiplexed shot, potentially being implemented in POC testing. It allows to estimate the disease severity in a patient or follow the behavior after therapy and intervention. Like other biosensors, electrochemical nanobiosensors function through (i) recognition of the analyte, (ii) signal transduction, and (iii) measurable signal readout. The first process relies on the bioreceptor-analyte interaction (Figure 2). The bioreceptor is any biological entity, usually live-derived (e.g., proteins as antibodies or cognate receptors, glycans, nucleic acids, whole cells), linked to an electrode previously modified with a nanostructured material or composite. When the analyte is recognized, physicochemical changes occur on the transducer's sensing interface, interpreted as a measurable signal in a concentration-dependent manner [95]. Electrochemical biosensors measure changes in the transducers' electrochemical properties, including electron transfer, charge accumulation, among others. The most common arrangement to measure such changes is the typical three-electrode cell, a frequent format in commercial SPEs. It uses a central working electrode (WE), where the biorecognition element is linked and the bioreceptor-analyte interaction occurs. Ideally, the WE is made with a conductive (or semiconductive) material (e.g., Pt, Au, C, semiconducting polymers), modified with nanostructures in the case of nanobiosensors (e.g., nanoparticles (NP), graphene, carbon nanotubes). The reference electrode (RE) has a very stable equilibrium potential (e.g., AgCl/Ag) to control the WE′s potential. This explains why the applied voltage is typically reported compared to a specific RE (Figure 2). The auxiliary or counter electrode (CE), also built with inert materials, aims to complete the last half-reaction in a controlled manner, closing the circuit. After an electrode arrangement is immersed into a supporting electrolyte solution, the power source (i.e., potentiostatic/galvanostatic electrochemical workstation) is adjusted depending on the potential window of reactants and the desired measurement type. A sufficiently concentrated electrolyte is required to abolish migration (i.e., ionic solute movements by the action of an electric field). High electrolyte concentration, relative to the analyte concentration in solution, ensures that it is statistically more probable that the electrolyte migrates to the electrode surface for charge balance. The applied potential (E) induces a heterogeneous electron transfer (hET) from the

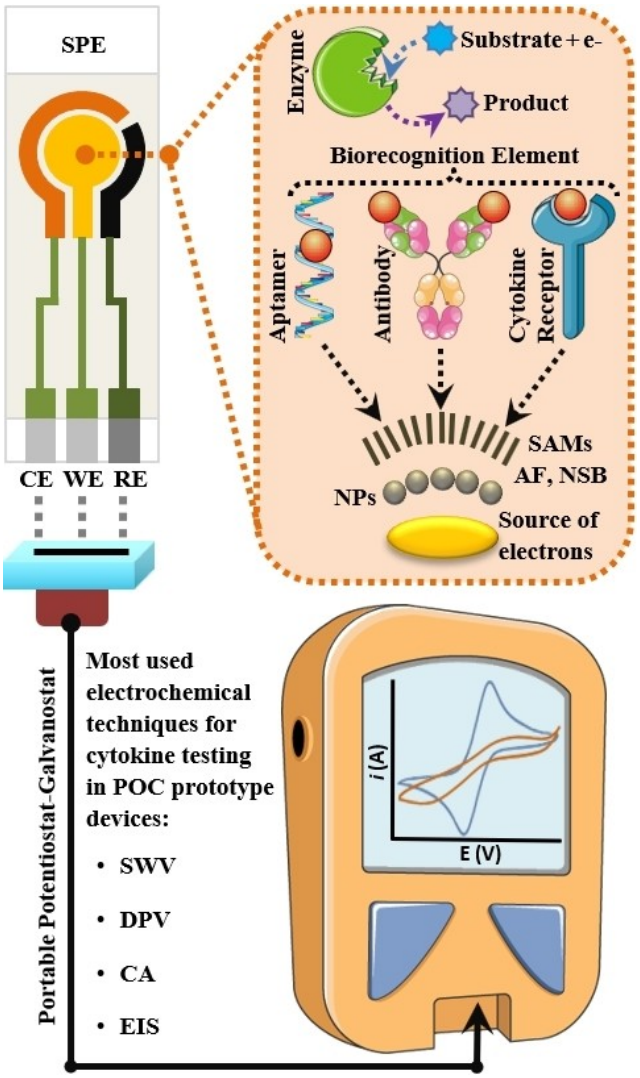

Fig. 2. General components and strategies for assembling electrochemical nanobiosensors based on screen-printed electrodes (SPEs). See the text for a detailed discussion. **CE:** Counter electrode; **WE:** Working electrode; **RE:** Reference electrode; **NPs:** Nanoparticles; **SAMs:** Self-assembled monolayers; **AF:** Antibiofouling; **NSB**: Nonspecific binding; **POC:** Point-Of-Care; **SWV:** Square wave voltammetry; **DPV:** Differential pulse voltammetry; **CA:** Chronoamperometry; **EIS:** Electrochemical-impedance spectroscopy. Some images were taken from free smart medical art.

WE to the CE, known as cathodic/anodic current (i). The electron flow provides the energy to oxidize or reduce electroactive molecules onto WE and CE, respectively. As the CE and RE events are so controlled, the WE redox phenomena are the only ones studied. In most cases, a tag is needed to produce a measurable hET, also known as faradaic current. Yet, free-label platforms are based on the fact that the bioreceptor-analyte union changes the transducer platform's electrical properties. Electrochemical biosensors can be classified depending on the signal measured onto the electrode from the biorecognition event, being amperometric, potentiometric, conductometric or impedimetric [96]. Among all interfacial electrochemical techniques, those controlling the potential while the current is measured ($i \neq 0$) are spread applied to tagged systems. Because three-electrode conformation is the most used arrangement, transduction for the cytokine biorecognition event onto its WE surface is usually determined by voltammetric techniques such as chronoamperometry, differential pulse voltammetry (DPV) or square wave voltammetry (SWV). Potentiometry and impedance-based techniques (e.g., electrochemical impedance spectroscopy, EIS; alternating current voltammetry, ACV) are mainly used in two-electrode label-free platforms. Even though the later techniques tend to be less applied with SPEs, they showed their usefulness to cytokines detection quickly and in real-time, as will be discussed.

One of the most common transducer platforms to construct electrochemical nanobiosensors is the SPEs. They may be commercially acquired and offer the possibility to bespoke it *in-home* relatively cheaply and straightforwardly [97]. The manufacturing process uses a mesh screen mask with the desired pattern that is positioned over the printing substrate, such as ceramic, glass, transparent flexible plastic, or even paper. The latter substrate is attractive because its porosity improves both the usable surface and the liquid's wicking rate, depending on its pore size and thickness. The Whatman grade 1 chromatographic filter paper is widely used because it is almost totally composed of α-cellulose (>98 %), is ashless and has a uniform right pore size with an ideal low thickness. Commented features put aside significant amounts of required components (e.g., ink, wax) and make it easy to penetrates through, optimally outlining the hydrophilic electrode zone and surrounding hydrophobic zone in the biosensor. The electrodes relied on paper can also improve the wettability either in the 2D (stacked) and 3D (folded, origami-like) formats, showing advantages to eliminate interferents and separate the sampling from electrochemical measurements, respectively [98].

Important features and principal formats of paper-based SPEs for cytokine measurement were recently reviewed [99]. When the substrate material is selected, a rubber squeegee is passed over the mesh several times to force a liquid paste (i.e., ink) to put in contact. Mandatory components included in the electrode ink are (i) a powdered metallic (e.g., Ag, Au, Pt) or nonmetallic (e.g., graphite) conductor, (ii) a solvent (e.g., terpineol, 2-ethoxyethanol, cyclohexanone, ethylene glycol) that furnish an apt printing viscosity as well as improve the volatility for thermal curing, and (iii) a substance that refines the mechanical and binding properties (e.g., glass powder, resins, cellulose acetate) to the substrate [100]. Dielectric inks and non-conductive inks are also printed as layers between electrodes to eliminate the interferences between them. In the end, the deposited ink is cured by heat- or UV-light [101].

Even though patterns obtained by screen-printing reach resolution of 30–100 μm, it is lesser than that from inkjet (15–100 μm) and aerosol-jet (10 μm), which are more amenable for miniaturization. In short, SPEs are widely used because they are cost affordable and accessible to be scaled up for mass production, maintaining their electrochemical properties. The manufacturing process may be tailored to include other techniques (e.g., microfluidics, modification with nanostructures), refining features such as resolution and sensitivity, decisive features in cytokine interrogation, and reviewed in the following sections. Moreover, the required modules to connect commercial or homemade SPEs, for data acquisition and the corresponding potentiostats/galvanostats are commercially available in portable formats to be used with a computer or a smartphone interface, facilitating (and accelerating) the POC testing approach (Figure 2).

2.1 Nanostructures as Enhancers of the Working Electrode Features

Understanding structures at the nanoscale (<100 nm) allows designing and synthesizing platforms over the working electrodes to enhance their performance. The optical, electrical, and magnetic properties may vary depending on the nanoscale's size, shape, and surface chemistry [102]. For instance, by the variation of gold nanoparticle (AuNP) shape (v.gr., nanospheres, nanostars, nanocubes, nanorods), a report proved that they absorb light sufficiently different in the presence of several bacteria (i.e., *E faecalis*, *E. coli*, *P. aeruginosa* and *S. aureus*), to be considered as a criterium for associating it to the presence of bacteria in a given sample [103]. Yet, for nano electrochemical devices, the interest falls over magnetic and electric properties. NPs can increase the available surface for biomolecules immobilization and the associated electroactive area of WE, leading to lower "overpotentials" and higher current densities in the resultant electrochemical biosensors. A large area also intensifies the scale of the redox conversion signal and the associated sensitivity, so if it is larger than the noise increase, the LOD is also improved. The higher resolution power conferred by the nanostructures is explained by its rapid hET rate capacity, featured by improved signals [104].

Regarding the shape, spherical NPs are virtually the only ones applied for cytokine biosensing platforms described in this review (Table 1) and others recently published [4,105]. Here, it is interesting to notice that multiplexed affinity biosensors (i.e., aptameric or immune sensors) based on wire-like micromotors may be used to accelerate the required testing time and to improve the LOD and LDR of the assays, as proven to other analytes [106,107]. Properties of magnetic NPs were applied mainly during analyte pre-concentration steps in electrochemical biosensors for cytokine sensing, with the consequent elimination or amelioration of the matrix effect (i.e., fouling and NSB) discussed below.

There are three main ways to modify the SPEs with a nanoparticulated system [108]: (i) drop-casting is the easiest because it requires the drop addition followed by drying selected NPs onto the WE. Carbonaceous nanomaterials functionalized with NPs (or nanocomposites) may be obtained *ex-situ* to control the final size better, avoiding agglomeration during drying. (ii) Electrodeposition induces the NPs formation by the application of a fixed potential (potentiostatic) or a constant negative current (galvanostatic), which reduces the precursor reagent (usually a metallic salt) up to achieving a zero valence. Tunning potential or current is made according to the used material and the desired size and shape of NPs. (iii) Ink-mixing and printing include combining NPs precursors with ink previously to curing. Since the ink-mixing manufacturing procedure implies all steps associated with the platform, it also requires a very sensitive control of variables to ensure its reproducibility (e.g., curing T°, mixing recipe, mixing methodology) to avoid NPs agglomeration. Therefore, generally preferred methodologies are drop-casting and electrodeposition after electrode aration, like most cytokine detection platforms.

As part of cytokine assessment, synthesis of NPs includes sources as noble metals (e.g., Ag, Au, Pt), Ruthenium (Ru), Nickel (Ni), Copper (Cu), TiO_2 (anatase) mesocrystal nanoarchitectures and polypyrrole nanoparticles. Most of them are based on Au and Carbon (C) derivatives like nanotubes in their conductive forms as either single-, dual or multiwalled forms (i.e., SWCNT, DWCNT, MWCNT), nanocomposites (e.g., AuNP/MWCNTs/chitosan, fullerene (C_{60})/CNTs) and reduced graphene oxide nanoparticles [105]. Back to the acceleration of the testing required time, graphene oxide rolled-up tubes with magnetic and catalytic movement [109] may improve the metrological features of cytokine's electrochemical nanobiosensors, mainly as preconcentration and anti-biofouling strategies.

2.2 Assembly of Cytokine Biorecognition Platforms for Electrochemical Biosensing

At this point, it should be clear that cytokines circulate at very low concentrations even if they are compared with hormones. Additionally, given the biological fluid complexity, cytokines coexist with many background components (e.g., albumin, other cytokines) that can be adsorbed onto the sensing interface or undergo a cross-reaction leading to nonspecifically hET (i.e., false-positive results). In this context, assembled platforms must possess a highly specific biorecognition element accompanied by other components that allow cytokine-dependent hET, impacting sensitivity and LOD. Tags are within the referred additional components (e.g., enzymes and nanozimes), mediators (e.g., tetramethylbenzidine, TMB; hydroquinone, HQ; methylene blue; MB) and antifouling materials (e.g., polyethylene glycol), all of them implemented to decrease the LOD and to increase or maintain the selectivity [110].

Table 1. Outstanding electrochemical biosensor platforms for the measurement of cytokine levels in a POC testing manner.

Cytokine	Platform	Method	Metrology	Ref.
IL-3	**Type**: Immunosensor **Electrode**: Gold AT (WE), Ag (RE), Gold AT (CE). **Nanostructure**: 2.7 μm Dynabeads M-270. **Functionalization**: NH– from Ab_1 reacts with epoxy groups over Dynabeads. **Detection**: Biotinylated anti-IL-3 Ab_2 reacts with streptavidin-HRP over WE.	**Sample**, **Time**, **T°**: Serum and whole blood (100 μL); ~1 h at 20 °C. **Equipment**: Custom-designed potentiostat. **Supporting solution:** pH 7.0 PBS. **Reactants**: H_2O_2 (substratum); Ultra-TMB (mediator). **Technique**: Chronoamperometry, 100 mV vs Ag/AgCl	**LOD**: 5 pg·mL^{-1} **LDR**: 5–10^4 pg·mL^{-1}	[116]
IL-6 **Other**: PSA, PSMA, PF-4.	**Type**: Microfluidic-based Immunosensor **Electrode**: Pyrolytic graphite (WE); 0.14 cm^2. **Nanostructure:** **1)** SWCNT forest over a thin layer of iron oxide-Nafion layer. **2)** 5 nm GSH-AuNPs over a positively PDDA charged surface. **Functionalization**: Imidization by EDC and Sulfo-NHS. **Detection**: Capture biotinylated anti-IL-6 Ab_1; Ab_2-streptavidin-HRP.	**Sample**, **Time**, **T°**: Serum (5–10 μL); ~3 h at 22 ± 2 °C. **Equipment**: Eight-electrode CHI 1030. **Supporting solution:** pH 7.0 PBS. **Reactants**: 0.4 M H_2O_2 (substratum); 1 mM hydroquinone (mediator). **Technique**: Chronoamperometry, –0.3 V vs SCE.	**LDR:** **1)SWCNT**: 40–150 pg·mL^{-1}. **2) AuNPs**: 10–4000 pg·mL^{-1}.	[158] [160] [192]
IL-6	**Type**: Aptasensor. **Electrode**: Au (WE; 1 mm ⌀), Ag/AgCl (RE), Pt (CE). **Nanostructure**: AuNPs (2–3 nm). **Functionalization**: Functionalized aptamer with alkanethiol HS–$(CH_2)_{11}(OCH_2CH_2)_3OH$. **Detection**: Aptamer against IL-6.	**Sample**, **Time**, **T°**: Commercial artificial sweat spiked with IL-6; ~1 h at 22 ± 2 °C. **Equipment**: Gamry 600 (Warminster, PA, USA). **Supporting solution**: 0.1 M PBS (pH 7.40) containing 5 mM $K_3Fe(CN)_6$. **Reactants**: None. **Technique**: EIS, 1 MHz to 1.0 Hz, 5.0 mV amplitude.	**LOD**: 0.02 pg·mL^{-1}. **LDR**: 0.02–20 pg·mL^{-1}.	[136]
IL-6	**Type**: Aptasensor **Electrode**: GCE (WE). **Nanostructure**: AuNPs **Functionalization**: pATP anchored by the amide bond on an electrochemically grafted pABA SAM. The COOH– was activated by NHS + EDC chemistry. **Detection**: Anti-IL-6 aptamer.	**Sample**, **Time**, **T°**: Serum from patients with colorectal cancer; ~1 h at $^{\circ}T_{Room}$. **Equipment:** **Supporting solution**: 0.1 M KCl containing 10 mM $[Fe(CN)_6]^{3-/4-}$. **Reactants**: None. **Technique**: EIS, 1 Hz to 10 kHz, with 10 mV amplitude.	**LOD**: 1.6 pg·mL^{-1}. **LDR**: 5–10^5 pg·mL^{-1}	[137]
IL-8	**Type**: Immunosensor **Electrode**: Reduced graphene oxide (WE), Pt (CE), Ag/AgCl (RE). **Nanostructure**: Cysteine capped Au NPs **Functionalization**: Imidization by EDC and Sulfo-NHS. **Detection**: Anti-IL-8 label-free.	**Sample**, **Time**, **T°**: PBS (Proof of concept) at $^{\circ}T_{Room}$. **Equipment**: Not provided. **Supporting solution**: PBS. **Reactants**: None. **Voltage**: 0.2 V vs Ag/AgCl **Technique**: Chronoamperometry	**LOD**: 0.589 pg·mL^{-1} **LDR**: 1–12 pg·mL^{-1}	[129]
IL-6 **IL-8** **Other**:	**Type**: Microfluidic-based immunosensor **Electrode**: **1)** Home-made SPE of Gold (WE; 0.42 mm^2 ⌀), wire Ag/AgCl (RE) and wire Pt (CE).	**Sample**, **Time**, **T°**: Serum (5 μL); 50 min at ~22 ± 2 °C. **Equipment**: Eight-electrode CHI 1030.	**LDR:** **1)** 10–1300 fg·mL^{-1} for IL-6. **2)** 5–50 fg·mL^{-1}	[164] [165]

Table 1. continued

Cytokine	Platform	Method	Metrology	Ref.
PSA, VEGF-C	**2)** Carbon (WE), Ag/AgCl (RE). **Nanostructure**: AuNPs (5 nm) onto the WE with a poly(diallydimethylammonium-chloride) (PDDA) layer. **Functionalization**: Imidization by EDC and Sulfo-NHS. **Detection**: Ab_1 captures the IL-6/IL-8 form sample onto WE, which in turn serves as attach points for the anti-IL-6/IL-8 Ab_2-MgB-HRP bioconjugates.	**Supporting solution:** pH 7.0 PBS. **Reactants**: H_2O_2 (substratum); Hydroquinone (mediator). **Technique**: Chronoamperometry, −0.3 V vs Ag/AgCl.	for IL-6; 10–50 fg·mL^{-1} for IL-8.	
IFN-γ	**Type**: Aptasensor **Electrode**: Gold (WE; 1.6 mm^2 ⌀), Ag/AgCl (3 M KCl, RE), Pt (wire, CE). **Nanostructure**: None. **Functionalization**: Aptamer with a 5'-terminus C6-disulfide $[HO(CH_2)_6–S–S–(CH_2)_6$-linker is reduced with TCEP, before WE Au–S bond is induced overnight. **Detection**: Aptamer against IFN-γ labeled with MB.	**Sample**, **Time**, **T°**: RPMI medium supplemented with bovine serum; ~20 min at °T_{Room}. **Equipment**: CHI 842B (CHInstruments, Austin, TX). **Supporting solution**: Liquid phase of sample. **Reactants**: hET between WE and MB-tagged aptamer. **Technique**: SWV, −0.1 to −0.5 V vs Ag/AgCl.	**LOD**: 1 pg·mL^{-1} **LDR**: 1–160 pg·mL^{-1}	[138]
IFN-γ	**Type**: Immunosensor **Electrode**: Homemade SPE of graphene (WE), Ag/AgCl (RE), C (CE). **Nanostructure**: Graphene – aniline. **Functionalization**: Imidization by EDC and Sulfo-NHS. **Detection**: Anti-hIFN-γ label-free.	**Sample**, **Time**, **T°**: 2 µL of TCA treated serum; ~50 min at °T_{Room}. **Equipment**: SP200 BioLogic (Biologic Science Instrument, France), Autolab Electrochemical Analyzer (Ecochemie, Netherlands). **Supporting Solution**: 0.1 M KCl containing 5 mM $[Fe(CN)_6]^{3-/4-}$. **Reactants**: None. **Technique**: EIS, 10^1–10^5 Hz; with 10 mV amplitude.	**LOD**: 3.4 pg·mL^{-1} **LDR**: 5–1000 pg·mL^{-1}	[130]
IFN-γ	**Type**: Immunosensor **Electrode**: ITO modified with graphite-chitosan film (WE; 3 mm^2 ⌀), Pt wire (CE), SCE (RE). **Nanostructure**: GHS-AuNPs. **Functionalization**: Imidization by EDC and Sulfo-NHS. **Detection**: Anti-hIFN-γ label-free.	**Sample**, **Time**, **T°**: Serum; 2 h at 35 °T. **Equipment**: CHI-832 (Chenhua Instruments Co, Shanghai, China). **Supporting solution**: 0.1 M PBS – $[Fe(CN)_6]^{4-/3-}$, pH 7.0 **Reactants**: None. **Technique**: DPV, −100 to 400 mV vs. SCE, at 100 mV/s.	**LOD**: 0.5 pg/mL **LDR**: 5–4000 pg/mL	[132]
IFN-γ	**Type:** **1)** 16-plexed immunosensor coupled to microfluidic (commercially available). **2)** 8-plexed continuous in-line system. **Electrode**: Au (WE), Au (CE), Ag/AgCl (RE). **Nanostructure**: None. **Functionalization**: Cystein-labeled Fab′, anti-IFN-γ. **Detection**: Biotinylated anti-IFN-γ Ab_1 reacts with streptavidin-HRP, then the formed complex binds to the captured IFN-γ over WE.	**Sample**, **Time**, **T°**: **1)** Plasma, serum (40 µL); ~1 h at °T_{Room}. **2)** Plasma, serum (40 µL); ~8 min at °T_{Room}. **Equipment**: Custom-made electronic board. **Supporting solution**: PBS and plasma. **Reactants**: H_2O_2 (substratum); TMB (mediator). **Technique**: Chronoamperometry, −300 mV vs Ag/AgCl.	**LOD**: **1)** ~10 pg·mL^{-1}. **2)** 40 pg·mL^{-1} **LDR**: **1)** 10–1000 pg·mL^{-1}. **2)** 16–2048 pg·mL^{-1}.	[176] [177]

Table 1. continued

Cytokine	Platform	Method	Metrology	Ref.
IFN-γ	**Type**: Immunosensor **Electrode**: C (WE; 4 mm^2 ⌀), C (CE), Ag (pseudo-RE). **Nanostructure**: None. **Functionalization**: Electrografting of *p*-ABA followed by EDC/sulfo-NHS activation. **Detection**: Biotinylated anti-IFN-γ Ab_1 reacts with streptavidin-HRP, then the formed complex binds to the captured IFN-γ over WE.	**Sample**, **Time**, **T°**: Undiluted saliva (5 µL).; ~2 h 30 min at °T_{Room}. **Equipment**: PGSTAT 101 for *p*-ABA grafting (Autolab), Autolab type III for EIS and CHI 1030B (CH Instruments) for amperometry. **Supporting solution:** pH 6.0 PBS. **Reactants**: H_2O_2 (substratum); Hydroquinone (mediator). **Technique**: Chronoamperometry, −0.2 V vs Ag pseudo-RE, for 5000 s.	**LOD**: 1.6 pg·mL^{-1}. **LDR**: 2.5–2000 pg·mL^{-1}.	[131]
TNFα	**Type**: Aptasensor **Electrode**: Gold (WE; 1.6 mm^2 ⌀), Ag/AgCl (3 M KCl, RE), Pt (wire, CE). **Nanostructure**: None. **Functionalization**: Aptamer with a 5'-terminus C6-disulfide [$HO(CH_2)_6$–S–S–$(CH_2)_6$-linker is reduced with TCEP, before WE Au–S bond is induced overnight. **Detection**: Aptamer against TNFα labeled with MB.	**Sample**, **Time**, **T°**: Drop of whole blood; ~20 min at °T_{Room}. **Equipment**: CHI 842B (CHInstruments, Austin, TX). **Supporting solution**: Liquid phase of the sample. **Reactants**: hET between WE and MB-tagged aptamer. **Technique**: SWV, −0.1 to −0.5 V vs Ag/AgCl	**LOD**: 10 ng·mL^{-1} **LDR**: 10–100 ng·mL^{-1}	[139]
TNFα	**Type**: Immunosensor **Electrode**: ITO (WE; 0.24 cm⌀), Pt (CE), Ag/AgCl (3.0 KCl; RE). **Nanostructure**: None. **Functionalization**: Electrografting in Ar atmosphere of PPC-PBA aryldiazonium salts followed by EDC/sulfo-NHS induces the attachment of the anti-TNFα (Ab_1). **Detection**: anti-TNFα (Ab_2) conjugated with HRP binds to the captured TNFα over WE.	**Sample**, **Time**, **T°**: Whole blood (40 µL).; ~1 h at °T_{Room}. **Equipment**: Autolab poten-tiostat (Metrohm Autolab) for electrografting, CV and CA; Solartron SI 1287 with an SI 1260 frequency response analyser (Hampshire, England) for EIS. **Supporting solution:** pH 7.4 PBS. **Reactants**: H_2O_2 (substratum); Ferrocene methanol (mediator). **Technique**: Chronoampero-metry, −0.05 V vs Ag/AgCl.	**LOD**: 10 pg·mL^{-1}. **LDR**: 0.01–500 ng·mL^{-1}.	[112]
TNFα	**Type**: Immunosensor **Electrode**: CSGM (WE; 0.24 cm^2 ⌀), Au (CE), Au (pseudo-RE). **Nanostructure**: Carboxylated magnetic nanoparticles (Sphereotech Inc, USA) sensitized with anti-Albumin and Anti-IgG for antifouling pretreatment step (i.e., NSB). **Functionalization**: Imidization by EDC and Sulfo-NHS. **Detection**: Anti-TNFα.	**Sample**, **Time**, **T°**: Undiluted serum (50 µL); ~2 h 30 min at °T_{Room}. **Equipment**: Reference 600™ (Gamry Instrument, USA). **Supporting Solution**: Redox probe 5 mM $[Fe(CN)_6]^{3-/4-}$ in 10 mM PBS, pH 7.4. **Reactants**: None. **Technique**: EIS, 0.5–500 KHz, with 25 mV amplitude.	**LOD**: 1 pg·mL^{-1}. **LDR**: 1–1000 ng·mL^{-1}.	[115]
TNFα	**Type**: Immunosensor **Electrode**: Au (WE; 7.07×10^{-2} cm^2 ⌀), Pt (CE), Ag/AgCl (3.0 KCl; RE).	**Sample**, **Time**, **T°**: Cell culture supernatants (10 µL).; ~20 min at °T_{Room}.	**LOD**: 0.1 pg·mL^{-1}. **LDR**: 1–150 pg·mL^{-1}.	[113]

Table 1. continued

Cytokine	Platform	Method	Metrology	Ref.
	Nanostructure: AuNPs-RGO nanocomposites. **Functionalization**: 4-aminophenyl held the AuNPs-RGO nanocomposites to WE. Electrografting of PPC-PBA aryldiazonium salts, followed by EDC/sulfo-NHS activation, induces the attachment of the anti-TNFα (Ab_1). **Detection**: anti-TNFα-ph-Fc-GO.	**Equipment**: CHI660E (CHI Instrument, Shanghai). **Supporting Solution**: Redox probe 5 mM $[Fe(CN)_6]^{3-/4-}$ in 10 mM PBS, pH 7.4. **Reactants**: None. **Technique**: SWV, −0.2 V to +0.6 V vs. Ag/AgCl, at 100 mV/s		
TNFα	**Type**: Aptasensor **Electrode**: C (WE; 12. 57 mm^2⌀), C (CE), Ag (pseudo-RE). **Nanostructure**: AuNPs. **Functionalization**: AuHCF-film-modified surface serves as AuNPs deposition via cyanide ions with the further thiolated aptamer reaction. **Detection**: Aptamer against IL-6.	**Sample**, **Time**, **T°**: Serum (50 µL).; ~20 min at °T_{Room}. **Equipment**: µStat DropSens potentiostat/ galvanostat (Drop Instrument; Spain). **Supporting Solution**: Redox probe 1 mM $[Fe(CN)_6]^{3-/4-}$ in 100 mM KCl, pH 7.4. **Reactants**: None. **Technique**: DPV, −0.1 to 0.3 V vs. Ag (pseudo-RE), at 10 mV/s.	**LOD**: 5.5 pg·mL^{-1}. **LDR**: 10–40 pg·mL^{-1}.	[140]
IL-1β **IL-6** **TNFα**	**Type**: Immunosensor **Electrode**: GC (WE; 0.071 cm^2⌀), Pt (CE), SCE (3.0 KCl; RE). **Nanostructure**: None. **Functionalization**: Electrografting of PPC-PBA aryldiazonium salts, followed by EDC/sulfo-NHS activation. **Detection**: Anti-IL-1β, anti-IL-6 and anti-TNFα secondary antibodies (Ab_2) labeled with GO-MB, GO-NB and GO-Fc, respectively.	**Sample**, **Time**, **T°**: Whole mouse serum (10 µL); ~30 min at °T_{Room}. **Equipment**: CHI660E (CHI Instrument, Shanghai). **Supporting Solution**: Redox probe 1 mM $[Fe(CN)_6]^{3-}$ in PBS buffer, pH 7.4. **Reactants**: hET induced by the redox reaction between WE, tags and Supporting electrolyte. **Technique**: SWV, −0.33 to −0.13 V for anti-IL-1β Ab_2-GO-MB; −0.58 to −0.3 V for anti-IL-6 Ab_2-GO-NB; 0.0 to 0.35 V for anti-TNFα Ab_2-GO-Fc; −0.6 to 0.4 V for simultaneous testing at 100 mV/s.	**LOD**: 5 pg·mL^{-1}. **LDR**: a) IL-1β: 5–200 pg·mL^{-1}; b) IL-6: 5–150 pg·mL^{-1}; c) TNFα: 5–200 pg·mL.	[114]

Ab_1: Primary antibody; **Ab_2**: Secondary antibody; **BSA**: Bovine serum albumin; **CE**: Counter electrode; **CSGM**: Comb structured gold microelectrodes arrays; **DPV**: Differential pulse voltammetry; **EDC**: 1-(3-(Dimethylamino)-propyl)-3-ethylcarbodiimide hydrochloride; **EIS**: Electrochemical impedance spectroscopic; **ET**: Electron transference; **$[Fe(CN)_6]^{3-/4-}$**: Solution 1:1 of $[Fe(CN)_6]^{4-}$ (ferrocyanide) and of $[Fe(CN)_6]^{3-}$ (ferricyanide); **Fc**: ferrocene; **GCE**: Glassy carbon electrode; **GO**: Graphene oxide; **GSH**: Reduced glutathione; **HFC**: Hexacyanoferrate; **ITO**: Indium tin oxide; **LDR**: Linear dynamic range; **LOD**: Limit of detection; the showed LODs correspond to cytokine only. **MCH**: Mercaptohexanol. **MgB**: Magnetic bead. **MB**: Methyl blue; **NB**: Nile blue; **NHS**: N-hydroxysulfosuccinimide; **NP**: Nanoparticle; **NSB**: Nonspecific binding; ***p*-ABA**: *p*-Aminobenzoic diazonium salt. **pATP**: p-Aminothiophenol; **ph-Fc**: 4-Ferrocenylaniline; **PBA**: 4-(4-aminoPhenyl) butyric acid; **PDDA**: Poly(diallydimethylammonium) chloride; **PF-4**: Platelet factor-4; **PPC**: 4-Amino phenyl phosphoryl-choline; **PSA**: Prostate-specific antigen; **PSMA**: Prostate-specific membrane antigen; **RE**: Reference electrode; **REF**: Reference; **RGO**: Reduced graphene oxide; **SAM**: Self-assembled monolayer; **SCE**: Saturated calomel electrode; **SPE**: Screen-printed electrode; **SWCNT**: Single-wall carbon nanotubes; **SWV**: Square wave voltammetry; **TCEP**: Tris-(2-carboxyethyl) phosphine**;** **TMB**: 3,3′,5,5′-tetramethylbenzidine; **TCA**: Tri-chloroacetic acid; **VEGF**: Vascular endothelial growth factor; **WO**: Working electrode.

In enzyme-labeled systems (e.g., horseradish peroxidase, HRP) for biosensing, the label's enzymatic activity gives an account of the bioreceptor-analyte recognition event. In first-generation enzymatic biosensors, the hET is promoted after the enzymatic products diffuse toward the WE by exchanging electrons. Second-generation enzymatic biosensors use artificial electron mediators to communicate the enzyme's active center and the electrode, improving the hET rate. In third-generation, the electrode functions as a source of electrons for catalysis, without product or mediator diffusion requirements [96]. Mostly general, whether biosensors are categorized based on how the bioreceptor oncomes to the transducer surface, the electrochemical biosensors can be classified into three categories. In the first class, the bioreceptor is bounded or entrapped behind a selective membrane allocated over the WE. Biosensors containing a signal enhancer over the WE interface (e.g., polymer matrix), together with the bioreceptor, belong to the second category. Finally, the third class is featured by the bioreceptor's direct attachment to the electrode, wholly integrated into the electrochemical sensing element. The latter is generally applied to affinity biosensors because the biorecognition event does not necessarily imply catalysis, but it is mandatory for electrochemical signal production. Selectivity is defined as the device's ability to correlate a readout with a specific analyte's change into a sample. The affinity electrochemical biosensing approach is the most spread format to measure cytokines and, in principle, this may be based on naturally occurring (e.g., antibodies, cognate receptors) or synthetic (e.g., nanobodies, aptamers) molecules to face selectivity issues (see below), one of the main challenges for biosensor devices.

Besides the selectivity, antifouling materials also help to face other important metrological variables for SPE-based cytokines measurement as repeatability and stability [111]. Nonspecific (protein) adsorption (fouling) or binding (NSB) over WE are usually avoided by the use of bovine serum albumin (BSA) in most of here detailed SPEs and other similar platforms for cytokine biosensing (Table 1). Depending on test design, incorporated BSA during blocking steps may behave as a fouling interferent, reducing the target cytokine's direct contact with the immobilized bioreceptor, which may hinder the hET and the associated biosensor metrological performance (e.g., sensitivity, reproducibility, stability) [105]. For instance, BSA induces an impedance increase that may alter the EIS-based approach's reliability. In contrast, stacked ordered polar antifouling molecules at the WE surface lead to a steric suppression that decreases mobility and entropy. Some antifouling materials also tightly bound a water film (hydration layer) that imposes a physical and energetic barrier to NSB and fouling, retaining the capacity to specific binding of the biorecognition element [110]. Briefly, there are three major workflows to incorporate the non-fouling chemistry onto SPE-based (or any electrochemical) biosensor surface: (i) self-assembly: commonly by thiol derived organics bonding over a WE surface of a noble metal (e.g., gold); (ii) electrografting: is normally applied for reductive grafting of diazonium salts chemistry (e.g., 4-amine phenyl phosphorylcholine, PPC; 4-(4-aminophenyl) butyric acid; PBA) over WE of C, Au or Pt (the mechanism is discussed in 2.2.1); and (iii) polymerization (e.g., electropolymerization): (meth)acrylates are usually applied with easy control of thickness and density parameters. Antifouling strategies must be considered if the required time frame for assessment is sufficiently long to consider biofouling as an important source of "background noise," in other words, if it conduces to a hET above LODs. Sandwich-like type immunosensors are less affected by fouling than EIS label-free based ones because the added antifouling layers produce a high-impedance effect hindering the WE faradaic current flow [110,112]. An electrochemical immunosensor for TNFα biosensing reported by Jiang *et al.*, serves as an example (Table 1). The work was based on Indium Tin Oxide (ITO) WE. It showed a reliable performance with whole blood, demonstrating that antifouling abilities furnished by PPC were retained even after the conjugation of high levels of anti-TNF-α antibodies through PBA moiety, which was consecutively electrografted after PPC. A higher complex workflow, also based on PPC-PBA chemistry to immobilize nanocomposites made with AuNPs and reduced graphene oxide (RGO) onto the WE, showed that PPC anti-biofouling behavior was retained but also improved ten times the LOD, compared with the previously reported for these types of platforms (i.e., from 1 pg/mL to 0.1 pg/mL) (Table 1) [113]. The multiplexed arrangement showed a similar PPC antifouling performance, while PBA served as a reliable substrate for simultaneous immobilization of anti-cytokine antibodies (i.e., anti-IL-1β, anti-IL-6 and anti-TNFα) [114]. Commented antifouling 3-plexed platform resolved each analyte using three different redox probes (i.e., ferrocene, Nile blue and methyl blue) that reached maxima hET peaks from −0.6 to 0.4 V range when were simultaneously tested at 100 mV/s scan rate (Table 1). Other approaches based on magnetic beads have been used as a biological affinity anti-biofouling to preconcentrate the cytokines and eliminate the major interferents that avoid the use of BSA for NSB. For instance, a two-step methodology that used two groups of immunomagnetic beads eliminated the albumin and IgG from the whole serum first and then preconcentrated the TNFα using a second set of magnetic beads. After the elution step with 2% SDS in 0.5 M Tris (pH 7.0) for 10 min at 63 °C, the assessment was done by EIS [115] (Table 1). The relatively high cost of the later methodology, joined to its impossibility to be carried out *in vivo*, constitutes its main limitation, but its reliability for POC testing was proven. In fact, in an outstanding work reported for IL-3 measurement in a POC testing manner, a similar system did include magnetic beads as preconcentration (and anti-biofouling) strategy (Figure 3A) (Table 1) [116]. The research idea was spined-off with the name of IBS (integrated biosensor for sepsis),

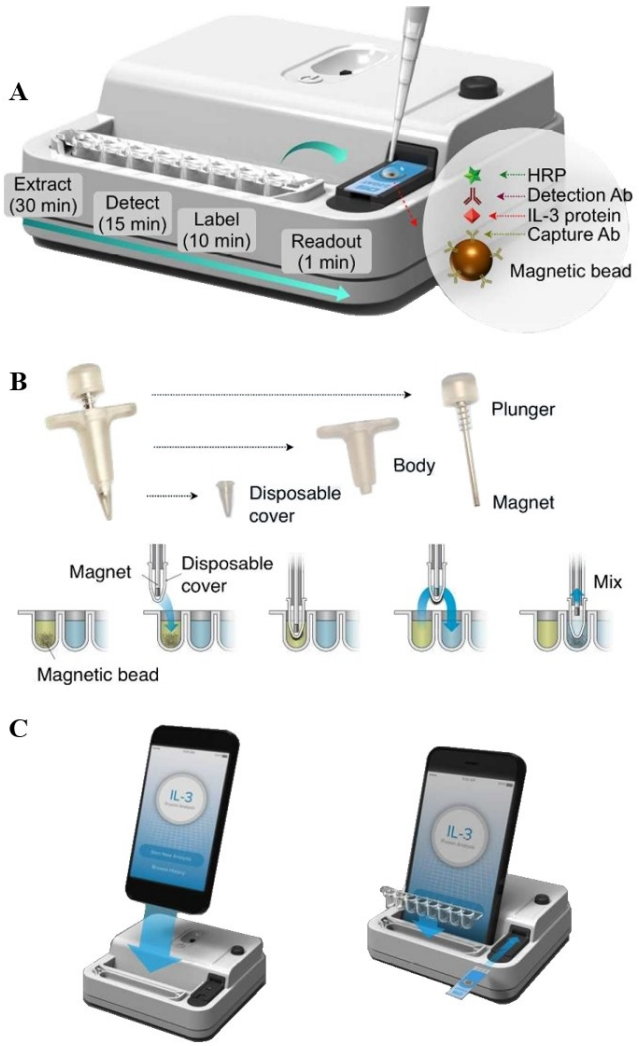

Fig. 3. Integrated biosensor for sepsis (IBS) relied on SPEs. The portable assay schematic (A) is based on a preconcentration system of Anti-IL-3 onto magnetic beads. The latter are mixed directly with plasma or whole blood and horseradish peroxidase (HRP)-labeled antibodies, which in turn are recovered by a plunger (B). The enzymatic reaction is read by chronoamperometry at the base station and interpreted by a smartphone app (< 1 h) (C). Reprinted by permission from [111].

permitting an accurate estimation of IL-3 concentration as sepsis diagnosis (Figure 3B). The use of a Bluetooth integrated into the miniaturized potentiostat served as the vehicle of information transfer from SPE readout to a smartphone (or laptop), where an app does process and transduce the chronoamperometric readout into concentration values (Figure 3C). The commented platform has a cost of goods of ~$50 for the IBS reader; the reagent cost was ~$5 per test and reached a LOD of ~5 pg/mL in whole blood after one h of testing, compared with the ~7 h required for IL-3 ELISA commercial kits ($11) or lateral flow strips ($10–20) [116]. Importantly, despite no report on any full anti-biofouling chemical effect in none platform, it may eliminate the need for cytokine sample pretreatment and open the door to *in vivo* continuous monitoring, a strategy that, nowadays, remains unexplored for cytokine biosensing (see 2.2.5. section). Other antifouling approaches based on porous electrodes, the use of membrane filters and self-cleaning membranes covalently modified with proteases (e.g., trypsin) are, in principle, also possible practical ways to restrict the interferent access to the underlying sensor. However, they were unexplored in SPE-based systems and the other formats for cytokine biosensors reviewed here.

2.3 Chemistry for Bioreceptor Immobilization onto the Working Electrode

Platform stability is one of the features desired when designing cytokines biosensors. This variable is mainly associated with the device's capacity to maintain the cytokine bioreceptor functional and attached to the solid WE surface or support. The last is true for SPEs, even if antifouling surface architectures are used. Thus, the ideal situation is when the biorecognition element's performance is not impeded by WE-associated additives (e.g., non-fouling supports). The immobilization of any biomolecule onto a flat WE may be accomplished randomly or site-directed. Adsorption is a random process that employs lesser material but typically has physisorption steps leading to denaturation, lower stability over time and less capacity to control the correct luminal exposition of the active binding sites.

Conversely, covalent bonding can improve the native folding maintenance and, in some cases, may lead to surface-oriented attachment onto the WE of the SPE. The most critical challenge in this field is to retain the anchorage points from the biorecognition system for their union to the analyte. For proteins, especially for antibodies, the primary amine groups are coupled to the sensor surface, pretreated with coating activators [117]. In general terms, there are three synthetic ways to orderly introduces each element to the system retaining its properties: (i) direct: both functionalities are inherently present in the same molecule (e.g., carboxybetaine thiol, oligo(ethylene glycol) thiol). (ii) co-incorporation: all the receptor, anchor and anti-biofouling separated units are present from begins. (iii) consecutive incorporation: activation surface step by self-assembly, electrografting or copolymerization, followed by bioreceptor immobilization, and spacers or antifouling with no functional moieties (e.g., sulfobetaine) to form the mixed interface. Despite the selected workflow, the bioreceptor: additive ratio must be optimized, especially in terms of density, by adjusting its concentration and immobilization time to guarantee the platform-analyte recognition capacity, with interfacial selectivity and antifouling behavior. The biorecognition elements used to estimate cytokines' concentration in a corporal fluid have been immobilized through plenty of surface chemistry procedures, but the most versatile for cytokine biosensing are described hereafter.

A self-assembled monolayer (SAM) is a 2D layer that appears after *n*-carbon atom alkyl chains containing

certain functional groups (v.gr. thiol, silanes), spontaneously reacts with electrode surface (e.g., Au, Pt), forming organic bonds and orderly deposits over the electrode area. The other extreme of alkyl molecules usually carries a moiety (e.g., –COOH) that serves as a reaction point for anchoring the biorecognition element (e.g., -NH_2). The high affinity of thiols for the common electrode materials leads to stable covalent bonding and simplifies the procedure for SAM formation. Therefore, n-alkanethiols compounds are widely used for surface functionalization in biosensors development [118]. Carboxylic acids are common functionalities introduced by 2-mercaptoethanoic acid, 3-mercaptopropanoic acid, glutathione and lipoic acid, but cysteine and its derivatives are also eventually used. The surface coverage of SAM is relative to its package level, chain length and charge density [119,120]. These variables may be controlled to modulate behaviors as quasicrystalline-like (e.g., 16-hexadecane thiol) or liquid-like (e.g., 16-hexane thiol), which in turn are a function of lateral interactions (e.e., hydrophobic, van der Waals, π-π) to confer stability. Notwithstanding, SAM-based immobilization is a random process that gives four conformations side-on, tail-on, head-on and flat-on, where the tail-on is the ideal. Some approaches are developed, searching a site-directed process in an oriented conformation (tail-on) [121]. Mostly, the SAM attachment procedure primes the electrode surface to the further immobilization of the bioreceptor. The first activation step of –COOH is usually made with 1-ethyl-3-(3-dimethylaminopropyl)-carbodiimide (EDC) as a crosslinker, followed by N-hydroxysuccinimide (NHS) to form an activated ester, a good leaving group. The bioreceptor's primary amines react with the activated sulfo-NHS ester, giving a stable conjugated amide bond. The methodology described above may be applied to bridge components as streptavidin or Fc binding proteins (e.g., A, G or L proteins), which serve as efficient side-oriented binding components for biotinylated enzymes, bioreceptors, antibodies, among others [122]. Other SAMs based on silanes (e.g., alkyl trichloro-, trialkoxy- or trichloro-silane) can be obtained to priming electrodes with an oxide layer (e.g., TiO_2) because it involves a nucleophilic attack of an activated hydroxyl group, but these are lesser or not at all used for cytokine biosensing [121]. The majority of works based on SPEs to assess cytokine levels, as described in this review, are based on thiolated SAMs.

Electrografting of diazonium salts (e.g., ArN^{2+}, p-aminobenzoic) had also been applied for cytokine biosensing. It begins from dissolving them into an acidic aqueous medium (e.g., sulfuric acid, H_2SO_4; 0.1 M) or an aprotic medium with a supporting electrolyte (e.g., a mixture of acetonitrile, CH_3CN, and tetra-butylammonium tetra-fluoroborate, NBu_4BF_4). After adding the above over the WE, the potentiostat is set at a negative potential enough to complete the reduction reaction. Polarized WE promotes the aryl group reaction with the electrode material (e.g., carbon-based, silicon, metal, indium tin oxide), forming a covalent aromatic organic layer. The very low cathodic potentials needed to reduce the diazonium salt onto the WE, plus the further attached aromatic ring with the starting amine, also made it favorable to use a wide range of substituents (e.g., alkyl, alkylated functions, ester, cyanide, halides, nitro, alcohols, thiols) by reduction. The reaction can be achieved quickly (min) and does not require dioxygen exclusion during assay when carbon-derived WE are used [123]. To create metal-carbon bonds, the WE must be free as possible from oxides, requiring to polish the surface prudently (to bar electrodes, but not to SPEs ones), which should be immediately followed by cleaning (rinse, sonication) and electrografting in deoxygenated conditions. The metal-aryl layer's covalent energy is probably greater than that reached by C or Si [123]. All quoted steps may also be done for electroaddressing, but, in this methodology, the receptor is previously functionalized with diazonium (e.g., 4-aminobenzylamine, 4-ABA; 4-aminobenzylamine, 4-ABA) and then electrochemically immobilized [124].

The tail-on configuration should be customized according to the bioreceptor nature. In the case of antibodies, site-oriented immobilization is achieved by its attachment through Fc components. Namely, Fc binding proteins, disruption of S–S bridges followed by sulfhydryl mediated attachment and oxidation of oligosaccharide Fc moieties coupled to amine or hydrazine terminated support [117,125,126]. In aptamers, it usually modifies an extreme that further reacts with a SAM or directly with the WE material (Table 1). Genetic engineering is also used to modify the naturally occurring receptor molecule with chelating amino acids as poly-His Tag, but this approach has been lesser explored in cytokines biosensing. The following presented electrochemical platforms for cytokines biosensing were done by applying the above-detailed surface chemistry.

2.4 Cytokine Electrochemical Immunosensors

Immunosensors use antibodies (Ab) as biorecognition elements. Abs are proteins with a "Y-like" form. The stalk of the "Y" is called the crystallizable fragment (Fc) region, and each arm is named the antigen-binding fragment (Fab) region. The distal part of Fab is variable and contains subregions known as paratopes, within which three complementarity-determining regions (CDRs) are found. Abs are conformed by four chains, two heavy and two light. There are two isotypes of light chains (i.e., κ, λ) and five isotypes of heavy chains which name to all antibody in its Latin form, to know, α (IgA), δ (IgD), ε (IgE), γ (IgG) and μ (IgM). Although most of them can be produced by plasma B cells to binds to any antigen (Ag), the most used isotype to modify the working electrode surface (i.e., capture Ab) and to detect the analyte (i.e., Ab_1, Ab_2) is the IgG. In outline, IgG highly undergoes mutagenic events that sharply upsurge the Ab affinity and complementarity, molecular variables that determine its specificity and selectivity level. Other isotypes' production requires additional genetic events

that complicate the *in vitro* synthesis. The immobilization of monoclonal antibodies enhances high specificity as a capture system (or like Ab_1). Polyclonal ones are better as detection strategy (Ab_2) in a sandwich-like format, heightening the sensitivity because a lot of tagged Ab_2 can react with Ab_1 increasing the signal. During Ab production, the Ag is processed to select the most immunogenic region as a target or epitope. Some cytokines have structural homology, which explains the cross-reactivity of used antibodies to detect them, mainly in the multiplexed approach, even if they are monoclonal.

The metrological effect of antibody-oriented immobilization seems to be less significatively in irregular 3D matrixes or is harder to clarify. In these platforms, randomly immobilized antibodies tend to be more significant than oriented ones [127]. Even though it is possible to use many electroactive probes held to Fc regions (e.g., ferrocene, anthraquinone, thionine, cobalt(III) bipyridine, $(Co(bpy)_3^{3+})$, $Ru(bpy)_3^{2+}$), the enzymes are the highest spread for electrochemical immunosensing (e.g., HRP) of cytokines. The chemistry of redox probes for Ab tagging to develop electrochemical immunosensors was recently published [128]. Likewise, Liu *et al.* expertly-reviewed the variables that affect the immunosensing process.

Recent work for IL-8 monitoring uses ivory paper to produce a WE by its immersion in graphene oxide solution followed by hydrazine reduction. Then, the reduced graphene oxide paper was electrophoretically modified with cysteine-capped gold nanoparticles (Cys-AuNPs) (Table 1) [129]. This system required neither tag nor mediator to complete the electrochemical monitoring of IL-8. Similar to later, a free-labeled platform for IFNγ was reported (Figure 4A) (Table 1) [130]. This label-free paper-based SPE was designed in a 3D origami format. They used Whatman filter paper grade 1 and graphene ink for screen-printing the WE. Electropolymerization of aniline did increase the electroactive area and introduced the amino moieties for the later immobilization of anti-hIFNγ mAb activated by the EDC/NHS chemistry. The IFNγ loading led to an increase in charge transfer resistance, measured by DPV, proportional to logarithmic concentrations of this cytokine (linear dynamic range (LDR) 5–1000 pg mL^{-1}, LOD 3.4 pg·mL^{-1}). Despite its low cost and good metrological performance, the commented system requires a trichloroacetic acid (TCA) precipitation step to eliminate the unwanted proteins decreasing its reliability by non-expert users. Better LDR was achieved by the use of more expensive substrates and NPs. For instance, a commercial carbon SPE was modified with an anti-IFNγ capture antibody through diazonium *p*-aminobenzoic salt (Table 1). This system measured amperometrically the IFNγ levels in saliva samples reaching better metrological specifications than the former one (LDR 2.5–2000 pg·mL^{-1}, LOD 1.6 pg·mL^{-1}) (Figure 4B) [131].

Likewise, the WE with self-assembled graphene/chitosan composite film over an ITO glass as a substrate was fabricated by screen-printing (Table 1) [132]. The

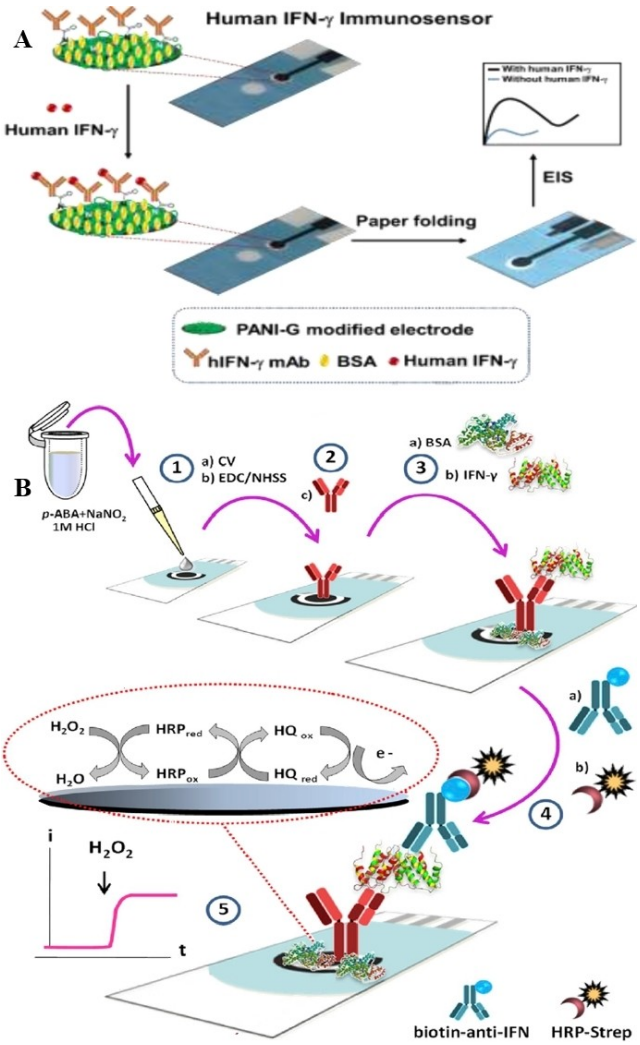

Fig. 4. Two immunosensors based on SPEs for IFNγ determination. Impedimetric format suggests the possibility of avoiding the use of labels to measure the IFNγ in serum (A). Amperometric immunosensor may be carried out in saliva in < 1.5 h (B). See the text for more details. Reprinted by permission from [130] and [131].

further modification with glutathione-protected gold nanoparticles (GSH-AuNPs) allowed to reach better sensitivity and a wider LRD (5–4000 pg·mL^{-1}; LOD 0.5 pg·mL^{-1}) for IFNγ testing in non-treated serum samples, compared with the commented formerly. Since the screen-printing have a limited resolution, some researchers had focused on microfabrication by lithography. Recent work showed the usefulness of an 8-WE immunosensor built onto a silicon wafer needle (Table 1). The platform included the immobilization of anti-IL-6 by a SAM of 6-mercapto-1-hexanol and the further assessment of IL-6 by DPV. In principle, the obtained platform may carry out the tests in solid tissues in real-time (~2.5 min) because of its needle shape (240-μm-wide, 2.1-mm-long, 40-μm-thick) instead of the typical blood

sampling [133], being useful to be implemented in future POC testing approaches.

2.5 Cytokine Electrochemical Aptasensors

Aptasensors rely on molecules termed aptamers, which can be synthesized from nucleic acids or peptides. Notwithstanding their biochemical nature, these molecules are characterized by their capacity to bind to a specific target molecule in a spread size range (e.g., ion, protein, intact cells), which explain its name (Latin′ *aptus*′, to fit; Greek ′meros′, part). Simultaneously discovered in the 90′s decade by Larry Gold and Jack Szostak's groups, they are regularly synthesized by a combinatorial chemistry technique, the systematic evolution of ligands by exponential enrichment (SELEX). Through this technique, the 3D conformation is gradually adjusted to the target shape by repeated cycles of selection (affinity) and synthesis (polymerase chain reaction) from a plethora of random sequences that show union activity for almost any kind of analyte with different intensity. The above increases the aptamer population that properly attains the different regions of the target binding molecules. High binding affinity towards analyte is mediated by structural complementarity and typical molecular interactions (e.g., electrostatic, stacking interactions, hydrogen bonds). The main aptamers′ success is that their targets′ nature is virtually irrelevant, in contrast with Abs that are recurrently synthetized just towards the most immunogenic regions of the processed molecule. Aptamer synthesis also has limitations as only 10^{14}, of a possible 10^{18}, of 20–60 mers are screened because of volume constraints, as well as that the used polymerases tend not to amplify secondary self-formed structures [3]. Once it is assembled, the electrochemical aptasensor-based measurement can proceed either in an off/on or an on/off manner. During the first one, the aptamers mediate the faradaic signal start upon binding its target, which is interpreted immediately by a transducer and displayed in a readout. Here, the reporters such as MB attached to the aptamer's extreme mediate a continuous low hET in the steady-state (off). The change in shape mediated by the analyte binding event comes to the reporter to a smaller distance from the electrode, leading to an increased hET rate (on).

In contrast, in the on/off format, the MB usually intercalates into dsDNA/dsRNA, generating a faradaic signal in the steady-state (on). Hence, the conformational changes of the aptamer shape, induced by the target bonding, release the reporter (or comes it in a long distance from the electrode surface), imposing a decrease in the hET rate in comparison with the steady-state (off), in such a way that the negative response is a function of the analyte concentration. Hitherto, the number of developed aptamers that can bind to different cytokines is limited. Besides, the sensitivity reached by electrochemical aptasensors for cytokines quantification is not sufficient to be applied to real samples. Moreover, given the great stability of aptamers, these platforms can be exposed to dissociation solutions to release the held cytokines allowing their reuse. The most important properties of aptamer-based biosensors have been reviewed elsewhere [134,135].

The IL-6 was assessed at sub-pM LOD with a label-free electrochemical nanoaptasensor through impedimetric measurement in artificial sweat (Table 1) (Figure 5A) [136]. Likewise, other works have shown good results for IL-6 detection in serum from patients with colorectal cancer (Table 1) [137]. Since the former has a better LOD ($0.02\ pg\cdot mL^{-1}$) and a closer LDR ($0.02–20\ pg\cdot mL^{-1}$) than the latter one ($1.6\ pg\cdot mL^{-1}$; $5–10^5\ pg\cdot mL^{-1}$), it is ideal for comparing the measurement in ultrafiltered body fluids as tears or sweat, with its usefulness in serum. Note that the assessment in ultrafiltered fluids is less invasive but, in this context, it is challenging to differentiate the paracrine

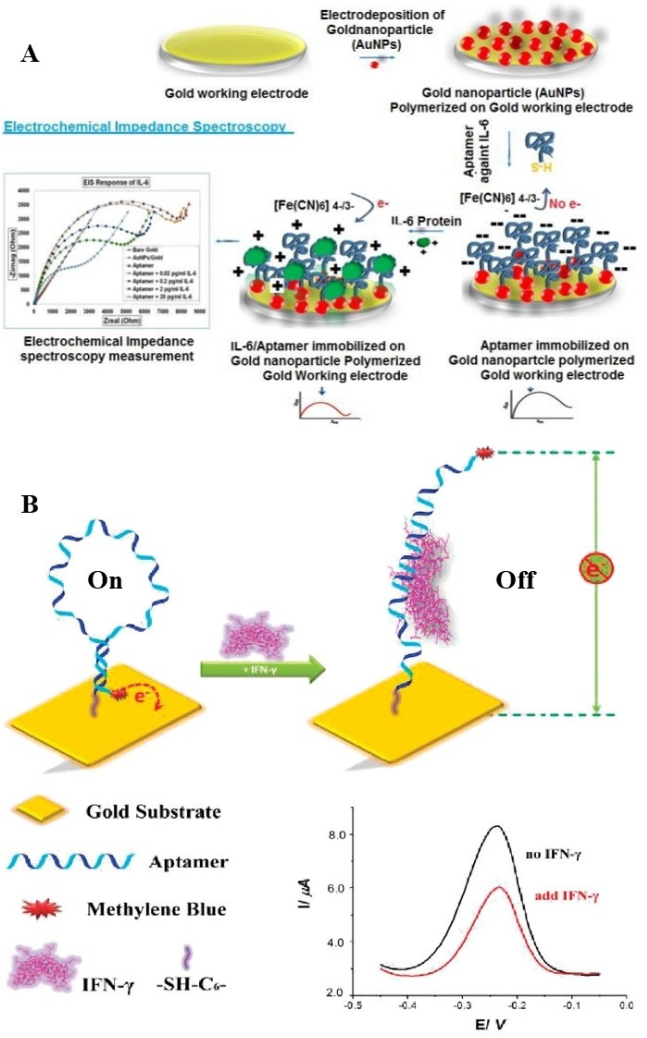

Fig. 5. Two aptasensors linked to SPEs with potential use for IL-6 and IFNγ determination. Impedimetric aptasensor may be carried out in sweat in ~1 h (A). The on/off format avoid the use of enzyme labels to measure the IFNγ in samples like serum (B). See the text for more details. Reprinted by permission from [136] and [138].

from the endocrine effect of IL-6. Amperometric aptasensors in the on/off format for cytokine measurement in complex samples had confirmed the usability of switching behavior of aptamer tagged with redox probes (e.g., MB, anthraquinone, ferrocene). Aptamers modified with 3'-MB were produced to react with both TNFα and IFNγ, showing that they could hold them when serum or whole blood were added directly onto gold WE, previously sensitized by Au–S surface chemistry (i.e., C6-disulfide [$HO(CH_2)_6$–S–S–$(CH_2)_6$–] linker) (Table 1) (Figure 5B) [138,139].

As with any on/off electrochemical aptasensor, the cytokine union decreased the faradaic signal, which can be followed by SWV. Later commented formats may be difficult to be repeated in SPEs because of strong conditions for WE decoration (e.g., phosphine, "piranha" solution). Label-free nano-SPE aptasensor for TNF-α determination showed a comparable LOD with reported immunosensors but relatively low stability (i.e., a decrease of 5 % of initial faradaic peak, after ~7 days, at 4 °C) (Table 1) [140]. Interestingly, in a typical electrochemical cell, LDR was expanded in on/off MB-based platform instead of SPE. Iron (II, III) oxide (Fe_3O_4) NPs coated with gold were decorated with a thiolated DNA probe, which in turn was hybridized with an aptamer against TNFα tagged with MB. The resulting composite (Fe_3O_4@AuNP-DNA duplex) was magnetically attracted on a glassy carbon WE, registering hET peak decrease after sample incubation because TNFα from serum competed for aptamer with the first DNA probe, being released (off) from the surface.

The later format did reach a wider LDR of 10 pg/mL to 100 ng/mL [141]. The development of aptasensors for cytokines also enables, in principle, real-time monitoring [142]. Several works at Prof. Plaxco's research group suggest that electrochemical aptasensors based on the typical three-cell electrode arrangement may carry out rapid readings (~4 s) of some drugs (e.g., vancomycin, tobramycin, gentamicin, doxorubicin), measured by SWV (Figure 6A) [143]. Similarly, the ratio between basal current registered at a not significant clinical concentration ($i_{non\text{-}responsive}$) and i_{min} also behaved as a proportionality constant (α) (Figure 6B) [147].

Most Plaxco approaches modified a roughened electrochemically gold wire electrode (e.g., 0.5 M sulfuric acid, 0–2 V vs Ag/AgCl) with 5'-aptamers through 6-mercapto-1-hexanol in PBS. To do that, DNA was reduced previously with tris (2-carboxyethyl) phosphine [144]. Finally, the electrode could be covered with a microporous 0.2 μm polysulfone membrane to shield the sensor from the background and mechanical fouling produced by blood cells [145]. Briefly, as the 3'-termini of the aptamer was modified with a redox reporter molecule (e.g., blue methylene), the electron transfer was a function of its distance to the WE surface (e.g., gold). Once the analyte bond, the change of aptamer conformation broth the reporter closer to the electrode, accelerating the hET with an intensity that depends on the applied

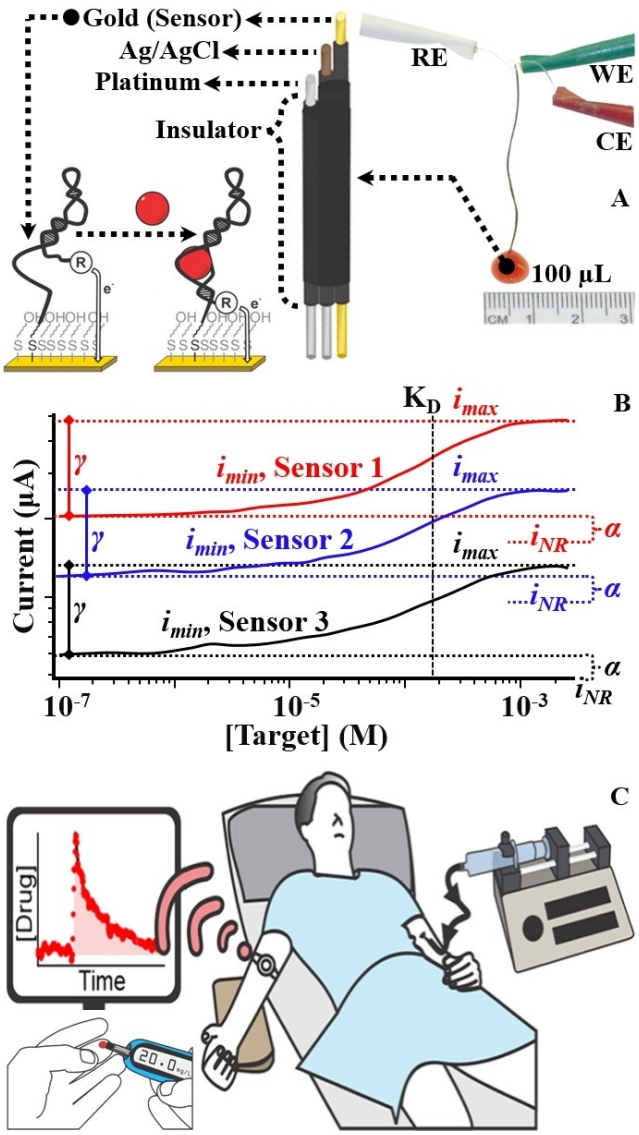

Fig. 6. Prototype aptasensor for continuous real-time measurement at POC from Prof Plaxco's lab (A). Three independently hand-fabricated cocaine-detecting sensors shown that the ratio between maximum and minimum currents (i_{max} and i_{min}) obtained from undiluted blood serum (denoted as γ) remains constant, as does the proportionality constant (α; relates i_{min} to non-response current, i_{NR}) and aptamer affinity, K_D (B). The later feature eliminates the calibration necessity and opens the possibility to produce automated POC electrochemical devices coupled to treatment (C). Reproduced with permission from [143] and [147].

square wave frequency during SWV [143]. Hence, as relied on the hET kinetics dependency of electrochemical aptasensors, the presence of target can be associated with a "signal-on" behavior (positive gain, in which binding causes a current increase) and a "signal-off" behavior (negative gain) by altering the applied square-wave frequency into a clinically relevant range of concentrations in undiluted flowing whole blood [146]. The approach of Dr. Plaxco's lab shows two full advantages. The system does not need calibration into effective

clinical range for some antibiotics. It was demonstrated that, despite the registered maximum and minimum currents (i.e., i_{max} and i_{min}) varied significantly from the sensor-to-sensor lot, their ratio (represented by γ) remained constant. (Figure 6B). Then, they used the output at the nonresponsive frequency together with γ, α and the dissociation constant of the aptamer (e.g., ~0.1 μM for vancomycin) for determining the analyte concentration in a methodology called kinetic differential measurements (KDM) [143]. Consequently, in the context of therapeutic drug monitoring, the described platform confers a second advantage: to adjust drug dosing *in situ* and real-time manner (~30 mins) from a continuous assessment of its concentration into flowing blood. In the end, the therapeutic drug window was maintained without causing significant adverse drug reactions [148], either in an anesthetized state [144,143] or in awake Sprague–Dawley rats [145].

Although these assays were made with relatively small molecules (e.g., vancomycin, kanamycin, cocaine) compared with cytokine, this kind of works emphasizes the importance of developing cytokines *in vivo* real-time measurements. They may be coupled to a simultaneously anti-inflammation treatment (i.e., theragnostic), depending on how their levels vary during a time, not only when they suddenly increase like storm cytokines in severe COVID-19 (Figure 6C) [58], but also when they decrease as a consequence of treatment. Finally, although Plaxco's electrochemical aptasensors are not based on screen-printing, the above-detailed nano-SPEs for cytokines' biosensing suggest the possibility to assemble any with comparable results.

2.6 Electrochemical Biosensors Based on Cytokine Cognate Receptors: An Innovative Door to be Opened

The cytokine cognate receptors must be highly specific because they must avoid the cross-reaction with other structural-related cytokines present in the extracellular space. In principle, it is possible to immobilize any kind of protein on the electrode surface, but variables as correct orientation and high coverage are critical. Assuming that those variables are surpassed, the high selectivity and specificity conferred by the cognate receptors could allow developing online/real-time formats, for example, by using the non-faradaic EIS. The electrode surface is exposed to charging and discharging cycles by applying alternating current (AC). Meanwhile, the dielectric changes are assessed as a function of the double-layer induction and its associated capacitance. Succinctly, the non-faradaic testing interprets the analyte biorecognition event mainly as a function of the transducer (electrode) capacitance.

In consequence, it tends to be less sensitive than faradaic EIS. Non-Faradaic biosensors require neither redox couples nor reference electrodes nor direct current. The latter property does not denature the immobilized receptor, maintaining its biorecognition capacity longer.

Two cell-based electrodes for non-faradaic EIS should be easily reduced in size and further installed in any alive organism without invasive procedures to measure the levels of a single or a group of cytokines at any time and in a POC manner. It contrasts with the common idea that the multiplexing relied on electrochemical nanobiosensors is limited by the relatively reduced number of redox probes available to induce the hET as the reporting electrochemical signals [149]. Finally, the impedimetric platforms need to be adjusted depending on the electrode size scale. For example, it has been reported that electrodes with <50 μm diameter can undergo an improvement in its hET, decreasing the impedance after biorecognition of the analyte, a contrary behavior to the observed at larger scales which in turn it is probably associated with increasing the area by the SAM sensitization [133]. It reduces the reliability of EIS in miniaturized systems but opens the door to other electrochemical techniques as DPV, which may be rapid, label-free and are also more straightforward than EIS [133].

When this review was written, the first multiplexed electrochemical device for the cytokine measurement in a POC-manner was published by Prof Prasad's research group, which relied on non-faradaic EIS [150]. Shortly, a flexible nanoporous polyamide substrate was used to print two gold electrodes by e-beam cryo-evaporation. These WEs were sputtered with zinc oxide (ZnO) semiconductor nanofilm to improve the rearrangement of charges that compose the double layer formed in the polarized electrode-electrolyte solution interface. Then, the WE surface was pretreated with dithiobis (succinimidyl propionate) (DSP) crosslinker dissolved in dimethyl sulphoxide (DMSO) to immobilize antibodies against cytokines with pro- (IL-6, IL-8) and anti-inflammatory (IL-10) functions as well as to serve as biomarkers for bacterial sepsis (TNF-Related Apoptosis-Inducing Ligand, TRAIL) and viral infection (CXCL-10, also known as interferon gamma-induced protein 10, IP-10). After the sampling (plasma, <40 μL), a small AC input voltage (10 mV, 1 kHz) is set at the electrode for impedance response measurements. The immunorecognition of cytokines led to double-layer structure rearrangement, measured using a portable electronic device that transduces the electrical outputs, from non-Faradaic EIS, into processable concentration data through a software interface (2048-point discrete Fourier transform-based impedance analyzer). The product was named DETecT (Direct Electrochemical Technique Targeting Sepsis) sensor, which was based on a previously developed platform known as EnLiSense's Rapid Electro-Analytical Device (READ), developed for the analysis of other biomarkers such as cortisol [151] and parathyroid hormone [152]. DETecT reached a detection limit of ~1 pg/mL being accomplished in ~min after dropping undiluted plasma. For a total of $n=40$ clinical samples, the comparison with Luminex reference methodology showed a correlation above 0.96 for most analytes, except TRAIL (Pearson's $r=0.89$). So, in principle, DETecT can rapidly estimate the oscillations in patients

that course by a cytokine storm during infection (e.g., COVID-19) and early predict the severity and determine the type of microorganism. To know, neutrophil activation (>>IL-8), 48 h and 28-day early mortality (high IL-6 and IL-8 levels), immune suppression and fatal outcome (>>IL-10) [58]. As was discussed above, the later system's specificity may be enhanced by immobilized cytokine cognate receptors, improving the device's POC testing accuracy.

3 Microfluidic Adapted Electrochemical Nanobiosensors: Towards Automated POC Multiplexed Cytokine Measurement

The biosensor array approach increases the WE number in the SPEs to convert them into a multi-analytical system. Typically, the CE area is wider than the WE one to ensure that the reactions' kinetic onto WE is not limited or inhibited. If the CE area is smaller than the sum of WEs areas in a sensor array, the commented format imposes interference during current measurements within the CE. So, a greater individual CE and RE are required in those systems to reach acceptable repeatability. Leaving the CE and RE outside of the SPE, but connecting them to one signal output, may counteract the referred problem [153]. There are lesser versatile solutions, namely, (i) to use diverse redox couple onto each WE, (ii) to improves the conductivity of each WE with different conducting polymers and (iii) to modify the (semi)conductive material of each WE, into the sensor array, by any with a similar overpotential [154]. Individualized channel formats can bespoke to be used in a single output channel, eliminating any multi-channel electrochemical workstation requirements, but both the LOD and sensitivity tend to be limited [154]. The aim of applying microfluidics to a measurement device is to transport, mix, and process all required liquid components of an assay into microchannels that connect to a microwell for single analyte detection; a focusing also called lab-on-a-chip [155]. Thus, the microfluidic-based electrochemical devices can analyze very small quantities of a sample in a short time, avoiding the cross-reactions but maintaining the low cost, high resolution and sensitivity of nanobiosensors. Potentially, microfluidic gadgets have better performance in all related to washing and reagent addition steps and can be miniaturized, leading to the automated, self-contained appliance, optimal for POC diagnostic approaches without sacrificing their metrological advantages [156]. Microfluidic systems also do plausible real-time cytokine detection.

Prof. Rusling's laboratory did adapt their experience during the development of a device based on microfluidics and electrochemical biosensors for genotoxicity screening [157] to cytokine detection among other analytes (e.g., IL-6, H_2O_2) (Table 1) [158,159]. Because pathobiology and the treatment of several signs (e.g., oral mucositis) during several cancers (e.g., colorectal, gastrointestinal and prostate cancers as well as head and neck squamous cell carcinoma) include the activation of NFκB and the further synthesis and release of cytokines, they were proposed as biomarkers. The first platforms on cytokine detection rely on IL-6 detection alone [160] or simultaneously with other biomarkers (e.g., prostate-specific antigen, PSA; prostate-specific membrane antigen, PSMA; and platelet factor-4, PF-4) [158]. Electrode arrays were modified with SWCNT forest or AuNPs, conjugated with capture antibodies in a sandwich-like manner. Biotinylated anti-IL-6 antibodies did increase the detection signal and did enhance the sensitivity, giving 14–16 HRP-streptavidin tags complex, per union event. In the same line, further developments did use a microfluidic sealed channel, made of polydimethylsiloxane (PDMS), 1.5 mm wide, 2.8 cm long, with 63 µL in volume, which was positioned between two hard flat poly (methylmethacrylate) (PMMA) plates. Two holes at PMMA permitted the introduction of electrode wires (i.e., 0.6 mm for Ag/AgCl RE and 0.2 mm for Pt CE). Capture tosyl-activated magnetic microparticles (MP, Dynabeads®, 1 µm diameter), modified with tens of thousands of HRPs and detection anti-IL-6, were mixed in an offline manner with the sample. Then, they began to flow over a carbon screen-printed WE, previously modified with AuNP-anti-IL-6. This platform reached an LDR of 0.30–20 pg/mL (sensitivity µA cm^{-2}/pg mL^{-1}) and required low analysis time (1.15 h), as well as practically eliminated the non-specific binding of possible interferents because the off-line capture applied system [161]. Further, by adding a stirred capture chamber, the system was multiplexed (i.e., IL-1β, IL-6, IL-8, TNFα, CRP) and did turn the off-line to an in-line strategy, which was more rapid (~30 min) and sensitive (Figure 7A, B) [162,163]. From compact recordable discs (CD-R), the researchers also fabricated eight SPEs by transferring a previously designed pattern printed in wax paper applying heat and pressure. The final electrochemical immunosensor reached 10–1280 fg mL^{-1} LDR for a cost affordable and rapid IL-6 measurement (1.15 h; <$0.2 per chip) [164]. With the introduction of gold nanostructured sensors and massively labeled paramagnetic detection beads, used in an off-line manner, the researchers also improved the required time (50 min) and achieved attomolar linear ranges (i.e., 5–50 fg·mL^{-1}) for IL-6, IL-8, vascular endothelial growth factor (VEGF), and VEGF-C in serum [165]. Most of these works rely on the capacity of HRP to produce an amperometric reduction signal in the presence of H_2O_2 with quinone as a reporter (Table 1). All platforms made by Prof. Rusling's group showed a good correlation with ELISA. The produced bioelectronic platform had versatile applications, being thoroughly customizable and high throughput by changing the sensing electrode or linking it to preconcentration systems based on (magnetic) NPs and coupling it to a multielectrode arrangement (e.g., 256 WE, Figure 7C) [166].

This last feature was especially highlighted in cytokines because most of the tests require diluting the sample

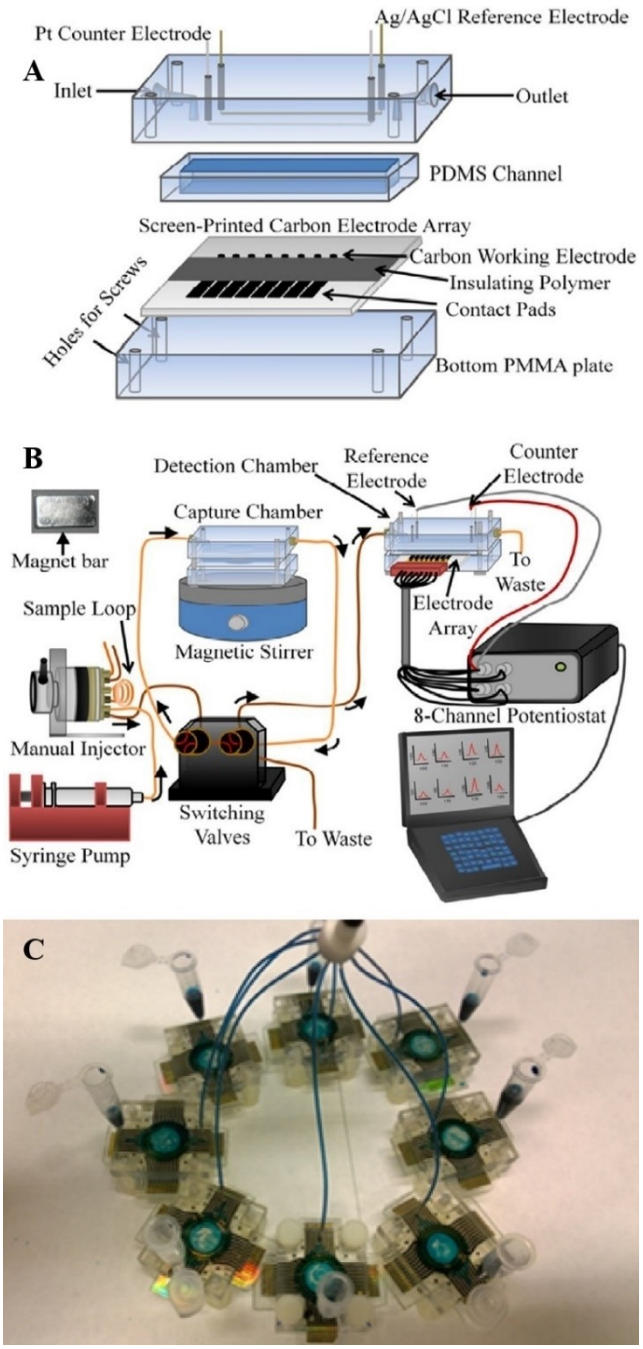

Fig. 7. SPE arrangements (A) coupled to microfluidics (B) from Prof Rusling's lab suggest the great potential of these kinds of systems to be multiplexed (C) in a miniaturized format for cytokine measurement at POC. See the text for more details. Reprinted by permission from [163] and [166].

to minimize or reverse the effect of soluble receptors or binding proteins that physiologically capture the cytokines, resulting in their low availability when tested [38,56]. Accordingly, the preconcentration systems relying on NPs, may help troubleshoot this problem by directly applying to whole samples, despite matrix complexity.

Lab-on-a-chip work of Prof. Revzin combines the electrochemical cytokine aptasensing with PDMS-based microfluidics for continuous *ex vivo* IFNγ measurement, without exogenous reagent requirements (Figure 8A, B) [166]. The early works demonstrated that it was possible to photopatterning the poly(ethylene glycol) hydrogel around the WE to simultaneously immobilize biomole-

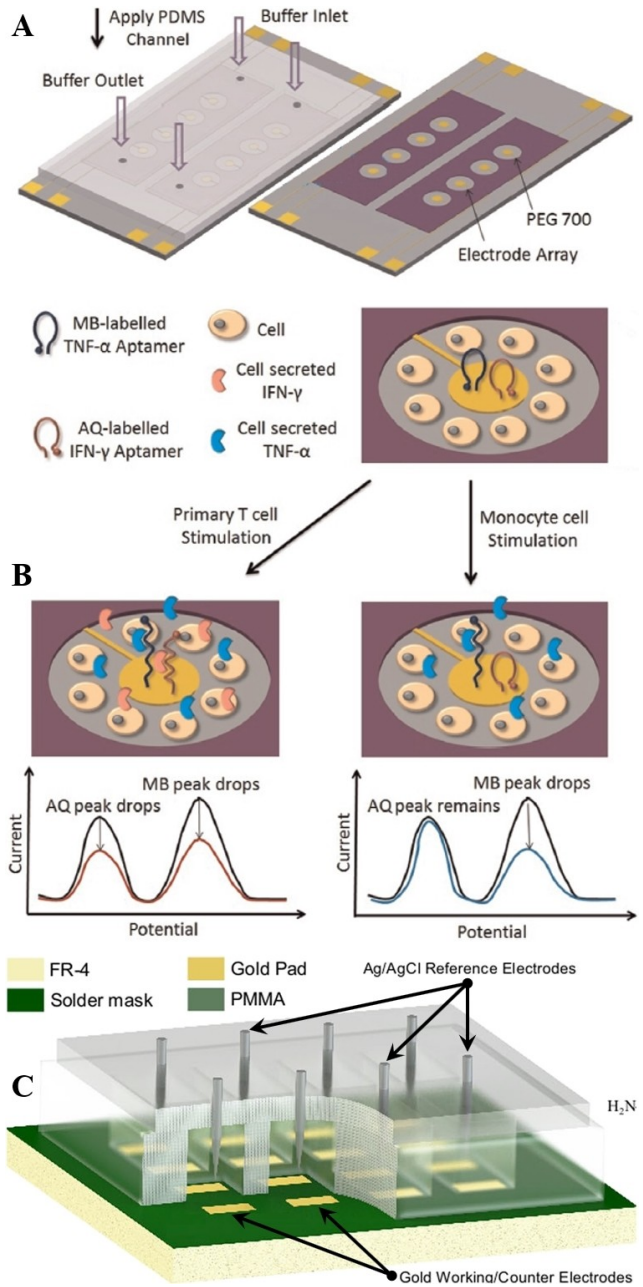

Fig. 8. Three electrode arrangement aptasensors coupled to microfluidics from Prof Revzin's lab (A). Its in-line format drove the sample to a magnet in the senor zone, where the IFNγ (or TNFα) presence was measured in an on/off manner (B). Another type of electrochemical device coupled to microfluidics for POC testing was developed by Prof Prodromakis' lab, which relied on printing circuit boards (C). See the text for a discussion in the context of SPEs. Reprinted by permission from [167] and [176].

cules like antibodies or enzymes (e.g., glucose oxidase, lactate oxidase) without affecting their activity [168]. Afterward, the early developed on/off aptasensors for IFNγ [138] and TNFα [139] were combined with a PDMS-based microfluidic system containing PEG-Anti-T cell capture hydrogel around WE [169,170]. The whole blood sampling through the inlet hole drove the leukocytes to the sensor zone, where T cells were trapped, allowing the simultaneous electrochemically biosensing of released IFNγ or TNFα cytokine in a continuous real-time manner [171]. Two-plexed systems were possible because of the distinct electrochemical behavior of a couple of redox probes for each cytokine aptamer (i.e., 5'-MB-TNFα and 5'-anthraquinone-IFNγ). Here, it is noteworthy that this system's capacity to trap circulating cells may be considered to appraise the yuxtacrine cytokine measurement, like mTNF, mainly as a POC approach. The simplistic architecture connects the sensor zone with the sampling channel, which has the inlet and outlet holes in both extremes. Further works included a magnet under the sensor zone for trapping magnetic beads sensitized with a 5'-ferrocene conjugated aptamer against IFNγ, via the non-covalent union biotin-3' to streptavidin present onto beads. Adsorbed nanocomposite initiates and maintains the hET (on) until the serum sampling drives IFNγ molecules to be held by the aptamer. The union event hindered the hairpin aptamer folding, moved the Fc redox tag away from the sensing interface and disrupted the basal faradaic current (off). The reached LDR (10–500 pg/mL) and LOD (6 pg/mL) contrasted with other microfluidic aptasensor-based electrochemical formats developed for continuous cytokine assessment in leukocyte cultures (e.g., LOD 1 ng/mL) [169]. Additionally, the later approaches can be introduced to evaluate the role of cytokines after mechanical injury in the POC approaches [172] or engineered tissue for toxicological evaluation, where the cytokines are usually monitored as damage grade biomarkers (e.g., irritant or corrosive) [173].

Professor Prodromakis' work has fallen over printing circuit boards (PCBs) instead of PDMS-SPEs in a different format. In this case, the microfluidic electrochemical biosensor cell for cytokine assessment (e.g., IFNγ) was obtained by commercially available PCB technology over tables made of flame retardant-class 4 (FR-4; 500 μm) (Figure 8C) (Table 1). Cycles of cooper etching with gold and silver allowed plating the WE, CE and RE in three staked layers, respectively [174]. The bottom layer contained the Au-based WE coupled to a microchannel network made of PMMA, etched by laser-assisted standard lithography [175]. Those microchannels interconnected the inlet and outlet, passing through the Au-CE (middle layer) and Ag/AgCl pseudo-RE (top layer) by the passive vertical interconnection access (VIAs) formats. An alternative format used a continuous flow in-line arrangement to test the analyte eliminating the incubation steps, but it needed a manual pump to introduce both samples and reagents, adding a variability that decreased the repeatability [176]. In the end, the amperometry measurements of IFNγ by the obtained PCB-based device reported a good correlation with commercial ELISA kit (R+D Biosystems). Both approaches used the HRP redox tag with TMB mediator by tracing the color change from blue to yellow after oxidation catalysis and the hET promoted by the redox reaction. Nevertheless, the device showed a sensitivity of 35 pg/mL for IFNγ colorimetric measurements, while no sensitivity was effectively reported for amperometric detection [177].

ELISA is commonly used for IFNγ measurement in diagnosing tuberculosis (TB) caused by the *Mycobacterium tuberculosis* infection. Preanalytical procedures imply the incubation of blood (~12 h) in the presence of TB antigens to stimulate the LT releasing of IFNγ. It is worth noting that lab-on-PCB device measurements used the plasma IFNγ spiked serum or plasma directly, assuming "high" IFNγ circulating levels in TB-suffering patients. However, as reviewed above, IFNγ is under melatonin/cortisol circadian control and tends to be paracrine, so preanalytical standardized sampling must be considered for its application (see below). Briefly, the Lab-on-PCB devices combined the electronic components, microfluidic systems control and electrochemical detection monolithically, which in turn has been proven only in combination with a commercially available IFNγ detection kit (R+D Biosystems) [176,177].

Microfluidic paper-based analytical devices (μPADs) may be SPE-like [178]. Millimeter-sized channels are patterned by photolithography. Starting from a hydrophobized substrate (e.g., paper immersed into octadecyl trichlorosilane or any ultraviolet resin), a previously designed microsized pattern (photomask) is transferred by its exposition to a UV-light source [179]. Once made, the hydrophilic zones for the flowing solutions path are parallelly outlined by hydrophobic walls that prevent the overflowing or backflowing from the paper sensor. The sample and reagents are guided by capillarity to individualized electrodes in a desired sensor array for testing. A particular advantage of a paper-based microfluidic system is that the transport through microchannels does not require any external driving force or pumping of reagents or samples [180]. The pores can serve as mesh during its flow, avoiding the sample pretreatment [98]. There are nine different techniques for μPADs fabrication, but the cheapest are inkjet-, wax-, screen- and laser-printing, in contrast with photolithography [179,181]. Renault *et al.* reported combining microfluidic systems patterned with photolithography and screen-printed carbon electrodes for unique and 18-plexed arrays [182]. Hitherto, the Renault-like systems have not been introduced to cytokines assessment. However, since they used bipolar electrochemistry, it does not require a direct electrical connection to a power supply to starts the faradaic processes, which may be a new scope to POC approaches for cytokines biosensing based on μPADs.

It should be quoted that the commercial microfluidic-based systems, or others applied to cytokine detections,

tends to be multi-analyte (single-plex) in contrast to multiplexed because they use a single channel-well to do the assay while avoiding cross-reactions. For instance, simple plex immunoassay cartridges from ProteinSimple use a detection platform built into glass nanoreactors allocated across individualized microfluidic channels. The workflow takes 1.5 h as reagents require to be pumped individually. A similar approach relied on mechanically induced trapping of molecular interactions (MITOMI) and used a freestanding button membrane triggered by pressure from a microfluidic device in a manner that sample or antibodies come in contact individually into membrane-wells allocated between the surface of an epoxy-silane coated glass slide and the PDMS-based chips, which should avoid the cross-reactions [183]. In principle, MIROMI technology can detect 384 biomarkers (i.e., 384 unique assays per device) in 2–3 h because the mixing is based on diffusion. Both above-presented cases have the same detection principle based on fluorescent-labeled antibodies, so the sensitivity is significatively affected by cross-reactivity, showing LDRs in pg/mL order [184,185].

In contrast, although some microfluidic coupled nano electrochemical biosensors have a multiplexed format, their LDRs tend to be in fg/mL order and are faster, as mentioned above. Theoretically, the latter properties can be upgraded by miniaturization because the assessment noise decreases as the electrode area does. So, the capacitive background associated with a thick charging double layer is minimized with smaller-sized electrodes. Closer distance between electrodes also minimizes the ionic path, leading to faster hET kinetics and reducing the Ohmic drop into the support solution furnished mainly by the uncompensated resistance (R_u).

All before commented electrochemical measurement equipment needs a very low quantity of energy, being portable and battery-operated. Moreover, its microfluidic design allows the continuous monitoring of cytokines in real-time, without adding exogenous reagents, even in the presence of overabundant serum proteins. If Prof. Rusling's and Prof. Revzin's microfluidic electrochemical arrangement detailed before are considered, others like Prof. Prodromakis' ones should be emulated or coupled to SPEs, despite themselves are not SPEs properly. Notice that all quoted features suggest that the POC biosensing platform for cytokines and other analytes is near to be feasible. Furthermore, the SPE-based technology may cost affordable and easy to handle in the clinical context.

4 Considerations for Optimal Sampling to Cytokines Measurement

The analytical variables and the sources of variation make difficult the measurement of cytokine levels. They include sample matrix effects, storage conditions (i.e., short or long term, liquid nitrogen or freezer), type of specimen (i.e., plasma or serum), choice of anticoagulants, within-subject temporal fluctuations, standardized reagents, platform type, laboratory procedures for accurate measurements, kit production lots, manufacturers, antibodies, and reference cytokines [74]. So, as with any test, it is mandatory to create broadly accepted laboratory practices to ensure cytokine measurement consistency, especially if new assay platforms are introduced [56,71]. In this context, an international interlaboratory program began in 2014 to identify variables that affect the Luminex bead-based cytokine assay outcomes, intending to create a routine proficiency testing that leads to harmonized protocols and quality improvements for this platform (https://eqapol. dhvi.duke.edu/programs/luminex) [186]. Likewise, researchers suggest that after obtaining the whole blood sample in endotoxin-free sterile tubes, immediately separate the plasma or serum from the cellular blood fraction and chill at 4 °C. Although most cytokines are conserved at −80 °C storage by 2 years, especially if the freeze-thaw cycles are avoided, they may be degraded after the first year (e.g., IL-13, IL-15, IL-17 and CXCL8) [56]. The mentioned technical steps should be ideally accompanied by some preanalytical considerations as a low-fat diet and exercise restrictions, as well as morning sampling, in a manner that all referred variability mentioned in the first part of this paper be limited, especially the matrix effect [56,62,70,187]. Additionally, it is mandatory to use pre-verified reagents or ideally from one manufacturer to avoid systematic errors [60,186,188,189]. The absolute values obtained by ELISA and multiplexed assays from the same vendor show the same tendency (i.e., low coefficient of variation) and a high value of intraclass correlation, but its scale can vary even in orders of magnitude [68]. Similar observations were obtained when either ELISA and multiplexed tests from different manufacturers were compared [69,188,189]. This explains why most commercial biotechnology brands that offer cytokine measurement kits suggest intra-assay levels [80]. Thus, some groups advise fixing the reference levels individually compared to the levels at the beginning of the study [149]. Despite the technical variability, it is clear that healthy individuals have differences in their basal cytokine levels compared with patients. In consequence, before the assessment, it is mandatory to determine what is the best sample (e.g., tears, saliva, serum, plasma, whole blood, blister fluid, etc.) to ensure the most identical conditions than may be possible either in sample processing or test performance [63,68,81,189].

5 Conclusion and Future Remarks

Commonly used multiplexed methods vary fundamentally in three features (i) degree of multiplexing (i.e., how many analytes), (ii) detection strategy (i.e., quantitative or qualitative) and (iii) throughput [75]. Therefore, considering the absence of the harmonized cytokine reference levels, together with their synthesis and consumption dynamics into a blood sample, developing POC systems

for cytokine multiplexed analysis is ideal, even in comparison with other protein biomarkers [190]. Electrochemical nanobiosensors and, especially SPE-based, are a promising option to be considered in cytokine measurement approaches. As it is well-known, the World Health Organization (WHO) numerates the ideal criteria to estimate any POC device's plausibility by using the acronym ASSURED. These properties should be optimally covered by electrochemical nanobiosensors for cytokine testing at the bedside, like those SPE-based, which do not require a conventional lab infrastructure. Ideal cytokine electrochemical nanobiosensors must accomplish several technological dispositions to be in line with the ASSURED criteria [111,169]: (i) Selectivity, a feature derived from the affinity and specificity conferred by the biorecognition element, which implies very low detection limit and low interferences (e.g., anti-biofouling), respectively. (ii) Metrologically defined as the calibration plot's slope (i.e., output/input signals), the sensitivity is crucial for useful cytokine biosensing (few $ml\,pg^{-1}$ or $ml\,fg^{-1}$ ideally). It is furnished by the electrode properties, as a high electroactive area and a proper density of well-oriented anchored bioreceptors, assuring a wide linear dynamic range. (iii) Fast responses into the temporal oscillations that are normal for cytokines (<30 min). This variable is associated with the electrode conductive properties and the electroanalytical technique applied to interpret the analyte presence. The response time progress is critical to developing devices capable of monitoring continually and in real-time the cytokines level during the disease course or therapy. (iv) Stability or long shelf life, a feature that primarily depends on conditions that maintain the biorecognition element attached to the electrode surface in a native form. After assembly, the storing conditions must be determined meticulously (e.g., T°, RH%). As stability is associated with repeatability (i.e., similar results among assays made in the same conditions), both variables make the devices more amenable to the market introduction. (v) Easy to be customized in miniature format, maintaining the same type of electrode's capacity to detect cytokines in a broad range of concentrations, either in one-by-one or in a multiplexed format. Such a feature facilitates industrial scalability. (vi) Cheaper than the commercial kits related to reagents, equipment, energy consumption and the possibility to be recycled. The conservation of electrode material during testing may be reduced by the thin layer of the conductive materials present in commercial SPEs electrodes (e.g., Ag made of RE), which is significantly degraded after a few cyclic voltammetry and series of impedance measurements [153]. (vii) Simplicity, in such a way that non-specialist users may operate them.

The effects of scarce commercial systems covering the above-stated conditions for cytokines determinations did rise during infections with SARS-CoV-2 pandemics. The necessity of a quick and straightforward way to measure pro-inflammatory cytokines (e.g., Il-1, IL-6, IL-8 and TNF-α) in a multiplexed manner has been one of the several crucial hindrances to avoid the severe phase of COVID-19 disease [4,150,191]. It is also worth noting that most of the electrochemical developments have been restricted to IL-6 and IFNγ, which has limited usefulness, considering the cytokine behavior, particularly their redundancy (i.e., shared effects between two or more cytokines) and synergy. In this regard, it is notable that the commercial multiplexed kits tend to show limitations for cytokines measurement from Th signature releasing profiles. For instance, compared with ELISA, multiplexed kits that included the cognate Th2 cytokine IL-5 have shown poor sensitivity [68], low correlation [63], unacceptably high CVs, or was undetectable in >50 % of the analyzed samples [69,70]. As was quoted in the first part of this review, IL-5 does not have important endocrine effects and is not expected to be found in the blood in normal conditions (<1 pg/mL). Consequently, ultrasensitive devices are needed for a reliable assessment of IL-5, as the other Th2 cytokines.

The potential for *in vivo* applications of electrochemical biosensors and the great sensitivity and specificity that may reach despite their simple format (e.g., nano-SPEs) contrasts with other POC testing methodologies [111]. For example, lateral-flow assays tend to be binary (i.e., presence/absence) and unstable in time, requiring exact time to be read and interpreted to avoid unspecific reactions and are lesser versatile for *in vivo* real-time applications. Overall, the versatility of the available biorecognition systems allows the production of analytic strategies for a wide range of targets, independently of its biochemical nature (e.g., Th2 cytokines).

The high electroactive area of the WE modified with nanostructures built from different materials makes nano-SPE electrochemical devices promising candidates to be used as cost affordable innovative cytokine bioassay tools, with simple operation, high sensitivity and specificity. Therefore, the reviewed biosensors may improve the yield of clinical processes in economic terms because it tends to eliminate the specialized requirements for diagnostic and treatment of many diseases (e.g., inflammation, sepsis, cancer), behaving as a complementary asset, like it has been discussed for other biosensors [193]. The significant required upfront investment and technical barriers are important hindrances for funding spin-offs based on this technology [194]. Commercialization efforts for the relative abundant research outputs on electrochemical nanobiosensors for cytokine detection in a POC manner are on the right path in both unique [116] and multiplexed formats [150]. The potential to incorporate the miniaturized electrochemical biosensors into microfluidic systems [163,166] may be amenable for further automation of devices either for POC testing [111] or for continuous wireless monitoring [143,147]. Thus, those features (i.e., miniaturization and microfluidic-coupled) are important technical challenges for scaling and commercializing any high throughput electrochemical biosensor [195]. Finally, it may be useful to apply NASA's Technology Readiness Levels (TRLs) criteria to estimate the grade of develop-

ment of a given biosensor platform to design the commercial strategy according to the idea (TRL 0–1), prototype (TRL 4–5), validation (TRL 6–7) and the final production and market phase (TRL 8–9) investment.

Acknowledgments

MINCIENCIAS has funded the work through Project Cod. 111584467470. J. O. thanks support from The University of Antioquia and the Max Planck Society through the cooperation agreement 566–1, 2014. E. P. thanks for support from The Institute of Chemistry, University of Antioquia. We thank The Ruta N complex and EPM for hosting the Max Planck Tandem Groups.

Data Availability Statement

All data presented in the present paper are reproduced with permission and available from the publishers listed in the respective figure captions.

References

[1] L. Muñoz, J. F. Contreras, O. Gutiérrez, P. T. Villalobos, L. G. Ramos, V. E. Hernández, in *Immune Response Activation and Immunomodulation, 1st ed.* (Eds.: R. K. Tyagi, P. S. Bisen), InTechOpen, London, **2019**, pp. 1–31.
[2] A. Zlotnik, *Front. Immunol.* **2020**, *11*, 908.
[3] A. P. Turner, *Chem. Soc. Rev.* **2013**, *42(8)*, 3184–3196.
[4] S. M. Russell, A. Alba-Patiño, E. Barón, M. Borges, M. Gonzalez-Freire, R. de la Rica, *ACS Sens.* **2020**, *5(6)*, 1506–1513.
[5] S. Campuzano, P. Yáñez-Sedeño, J. M. Pingarrón, *Sensors* **2021**, *21(1)*, 189.
[6] E. S. Baekkevold, M. Roussigné, T. Yamanaka, F. E. Johansen, F. L. Jahnsen, F. Amalric, P. Brandtzaeg, M. Erard, G. Haraldsen, J. P. Girard, *Am. J. Pathol.* **2003**, *163(1)*, 69–79.
[7] L. Roussel, M. Erard, C. Cayrol, J. P. Girard, *EMBO Rep.* **2008**, *9(10)*, 1006–1012.
[8] V. Carriere, L. Roussel, N. Ortega, D. Lacorre, L. Americh, L. Aguilar, G. Bouche, J. Girard, *Proc. Natl. Acad. Sci. USA.* **2007**, *104(1)*, 282–287.
[9] S. Ali, A. Mohs, M. Thomas, J. Klare, R. Ross, M. L. Schmitz, M. U. Martin, *J. Immunol.* **2011**, *187(4)*, 1609–1616.
[10] V. Gautier, C. Cayrol, D. Farache, S. Roga, B. Monsarrat, B. Burlet, A. Gonzalez, J. P. Girard, *Sci. Rep.* **2016**, 6, 34255.
[11] J. Travers, M. Rochman, C. E. Miracle, J. E. Habel, M. Brusilovsky, J. M. Caldwell, J. K. Rymer, M. E. Rothenberg, *Nat. Commun.* **2018**, *9(1)*, 3244.
[12] C. Cayrol, J. P. Girard, *Immunol. Rev.* **2018**, *281(1)*, 154–168.
[13] D. Brenner, H. Blaser, T. W. Mak, *Nat. Rev. Immunol.* **2015**, *15(6)*, 362–374.
[14] J. Holbrook, S. Lara-Reyna, H. Jarosz-Griffiths, M. McDermott, *F1000Research.* **2019**, *8*, F1000 Faculty Rev–111.
[15] G. D. Kalliolias, L. B. Ivashkiv, *Nat Rev Rheumatol.* **2016**, *12(1)*, 49–62.
[16] Y. Qu, G. Zhao, H. Li, *Front. Immunol.* **2017**, *8*, 1675.
[17] M. Grell, H. Wajant, G. Zimmermann, P. Scheurich, *Proc. Natl. Acad. Sci. USA.* **1998**, *95(2)*, 570–575.
[18] P. D. Hodgkin, J. Rush, A. V. Gett, G. Bartell, J. Hasbold, *Immunol. Cell Biol.* **1998**, *76(5)*, 448–453.
[19] G. Altan-Bonnet, R. Mukherjee, *Nat. Rev. Immunol.* **2019**; *19(4)*, 205–217.
[20] J. P. Girard, C. Moussion, R. Förster, *Nat. Rev. Immunol.* **2012**, *12(11)*, 762–773.
[21] O. Schulz, S. I. Hammerschmidt, G. L. Moschovakis, R. Förster, *Annu. Rev. Immunol.* **2016**, *34*, 203–242.
[22] L. B. Ivashkiv, *Nat. Rev. Immunol.* **2008**, *8(10)*, 816–822.
[23] D. R. Fooksman, S. Vardhana, G. Vasiliver-Shamis, J. Liese, D. A. Blair, J. Waite, C. Sacristán, G. D. Victora, A. Zanin-Zhorov, M. L. Dustin, *Annu. Rev. Immunol.* **2010**, *28*, 79–105.
[24] B. Alarcón, D. Mestre, N. Martínez-Martín, *Immunology.* **2011**, *133(4)*, 420–425.
[25] M. Fritzsche, M. L. Dustin, in *Structural Biology in Immunology, 1st ed.,* (Eds.: C. Putterman, D. Cowburn, S. Almo). *Academic Press*, Massachusetts, **2018**. pp. 1–37.
[26] M. Huse, B. F. Lillemeier, M. S. Kuhns, D. S. Chen, M. M. Davis, *Nat. Immunol.* **2006**, *7(3)*, 247–255.
[27] A. Onnis, C. T. Baldari, *Front Cell Dev Biol.* **2019**, *7*, 110.
[28] H. H. Jung, J. Y. Kim, J. E. Lim, Y. H. Im, *Sci. Rep.* **2020**, *10(1)*, 14069.
[29] J. A. Walker, A. N. McKenzie, *Nat. Rev. Immunol.* **2018**, *18(2)*, 121–133.
[30] W. E. Paul, J. Zhu, *Nat. Rev. Immunol.* **2010**, *10(4)*, 225–235.
[31] I. S. Junttila, *Front. Immunol.* **2018**, *9*, 888.
[32] S. J. Van Dyken, R. M. Locksley, *Annu. Rev. Immunol.* **2013**, *31*, 317–343.
[33] J. Zhu, *Cytokine.* **2015**, *75(1)*, 14–24.
[34] E. Patiño, A. Kotzsch, S. Saremba, J. Nickel, W. Schmitz, W. Sebald, T. D. Mueller, *Structure.* **2011**, *19(12)*, 1864–1875.
[35] F. Roufosse, *Front Med* (Lausanne). **2018**, *5*, 49.
[36] C. A. Dinarello, *J. Endotoxin Res.* **2004**, *10(4)*, 201–222.
[37] A. Blomqvist, D. Engblom, *Neuroscientist.* **2018**, *24(4)*, 381–399.
[38] S. A. Jones, S. Rose-John, *Biochim. Biophys. Acta* **2002**, *1592(3)*, 251–263.
[39] L. H. Calabrese, S. Rose-John, *Nat Rev Rheumatol.* **2014**, *10(12)*, 720–727.
[40] J. Wolf, S. Rose-John, C. Garbers, *Cytokine.* **2014**, *70(1)*, 11–20.
[41] H. Su H, C. T. Lei, C. Zhang, *Front. Immunol.* **2017**, *8*, 405.
[42] S. Rose-John, K. Winthrop, L. Calabrese, *Nat Rev Rheumatol.* **2017**, *13(7)*, 399–409.
[43] K. Urschel, I. Cicha, *Int J Interferon Cytokine Mediat. Res.* **2015**, *7*, 9–25.
[44] S. Bhatnagar, S. K. Panguluri, S. K. Gupta, S. Dahiya, R. F. Lundy, A. Kumar, *PLoS One.* **2010**, *5(10)*, e13262.
[45] C. A. Dinarello, *Eur. J. Immunol.* **2007**, *37 (Suppl 1)*, S34–45.
[46] P. Lissoni, F. Rovelli, F. Brivio, O. Brivio, L. Fumagalli, *Nat. Immun.* **1998**, *16(1)*, 1–5.
[47] N. Petrovsky, L. C. Harrison, *Int. Rev. Immunol.* **1998**, *16(5–6)*, 635–649.
[48] J. D. Scheff, S. E. Calvano, S. F. Lowry, I. P. Androulakis, *J. Theor. Biol.* **2010**, *264(3)*, 1068–1076.
[49] A. Nakao, *J Immunol Res.* **2014**, *2014*, 614529.
[50] S. M. Kim, N. Neuendorff, D. J. Earnest, *Sci. Rep.* **2019**, *9(1)*, 8909.

[51] A. Steensberg, C. Keller, R. L. Starkie, T. Osada, M. A. Febbraio, B. K. Pedersen, *Am. J. Physiol. Endocrinol. Metab.* **2002**, *283(6)*, E1272–8.
[52] J. W. Helge, D. K. Klein, T. M. Andersen, G. van Hall, J. Calbet, R. Boushel, B. Saltin, *Exp. Physiol.* **2011**, *96(6)*, 590–598.
[53] T. Matsuda, T. Hirano, S. Nagasawa, T. Kishimoto, *J. Immunol.* **1989**, *142(1)*, 148–152.
[54] J. LaMarre, G. K. Wollenberg, S. L. Gonias, M. A. Hayes, *Lab. Invest.* **1991**, *65(1)*, 3–14.
[55] C. L. Mack, *Hepatology.* **2007**, *46(1)*, 6–8.
[56] W. de Jager, K. Bourcier, G. T. Rijkers, B. J. Prakken, V. Seyfert-Margolis, *BMC Immunol.* **2009**, *10*, 52.
[57] E. Masselli, G. Pozzi, G. Gobbi, S. Merighi, S. Gessi, M. Vitale, C. Carubbi, *Cell* **2020**, *9(9)*, 2136.
[58] D. C. Fajgenbaum, C. H. June, *N. Engl. J. Med.* **2020**, *383(23)*, 2255–2273.
[59] V. V. Krishnan, R. Ravindran, T. Wun, P. A. Luciw, I. H. Khan, K. Janatpour, *Cytometry Part B* **2014**, *86(6)*, 426–435.
[60] J. A. Stenken, A. J. Poschenrieder, *Anal. Chim. Acta* **2015**, *853*, 95–115.
[61] N. Aziz, P. Nishanian, R. Mitsuyasu, R. Detels, J. L. Fahey, *Clin. Diagn. Lab. Immunol.* **1999**, *6(1)*, 89–95.
[62] K. T. Lappegård, M. Fung, G. Bergseth, J. Riesenfeld, T. E. Mollnes, *Ann Thorac Surg.* **2004**, *78(1)*, 38–44.
[63] H. L. Wong, R. M. Pfeiffer, T. R. Fears, R. Vermeulen, S. Ji, C. S. Rabkin, *Cancer Epidemiol. Biomarkers Prev.* **2008**, *17(12)*, 3450–3456.
[64] P. Riches, R. Gooding, B. C. Millar, A. W. Rowbottom, *J. Immunol. Methods.* **1992**, *153(1–2)*, 125–131.
[65] W. Seiler, H. Müller, C. Hiemke, *Clin. Chem.* **1994**, *40(9)*, 1778–1779.
[66] A. Gudmundsson, W. B. Ershler, B. Goodman, S. J. Lent, S. Barczi, M. Carnes, *Clin. Chem.* **1997**, *43(11)*, 2199–2201.
[67] P. W. Thavasu, S. Longhurst, S. P. Joel, M. L. Slevin, F. R. Balkwill, *J. Immunol. Methods* **1992**, *153(1–2)*, 115–124.
[68] M. F. Elshal, J. P. McCoy, *Methods.* **2006**, *38(4)*, 317–323.
[69] A. K. Chaturvedi, T. J. Kemp, R. M. Pfeiffer, A. Biancotto, M. Williams, S. Munuo, M. P. Purdue, A. W. Hsing, L. Pinto, J. P. McCoy, A. Hildesheim, *Cancer Epidemiol. Biomarkers Prev.* **2011**, *20(9)*, 1902–1911.
[70] A. Biancotto, X. Feng, M. Langweiler, N. S. Young, J. P. McCoy, *Cytokine.* **2012**, *60(2)*, 438–446.
[71] S. X. Leng, J. E. McElhaney, J. D. Walston, D. Xie, N. S. Fedarko, G. A. Kuchel, *J Gerontol A Biol Sci Med Sci.* **2008**, *63(8)*, 879–884.
[72] K. Hatta, M. J. Bilinski, J. K. Haladyn, J. J. Roy, J. Horrocks, M. J. van den Heuvel, V. K. Han, B. A. Croy, *Am J Reprod Immunol.* **2009**, *62(3)*, 158–164.
[73] H. K. Skalnikova, J. Cizkova, J. Cervenka, P. Vodicka, *Int. J. Mol. Sci.* **2017**, *18(12)*, 2697.
[74] J. W. Findlay, W. C. Smith, J. W. Lee, G. D. Nordblom, I. Das, B. S. DeSilva, M. N. Khan, R. R. Bowsher, *J. Pharm. Biomed. Anal.* **2000**, *21(6)*, 1249–1273.
[75] M. M. Ling, C. Ricks, P. Lea, *Expert Rev. Mol. Diagn.* **2007**, *7(1)*, 87–98.
[76] L. Castillo, D. M. MacCallum, *Methods Mol. Biol.* **2012**, *845*, 425–434.
[77] S. Khalifian, G. Raimondi, G. Brandacher, *J. Invest. Dermatol.* **2015**, *135(4)*, 1–5.
[78] N. I. Medeiros, J. A. S. Gomes, *Methods Mol. Biol.* **2019**, *1955*, 309–314.
[79] X. Le Guezennec, J. Quah, L. Tong, N. Kim, *Mol. Vision* **2015**, *21*, 1151–1161.
[80] P. Chapman, C. Reyes, V. Gupta, *BIORAD.* **2010**, Tech note *6029*.
[81] A. Biancotto, A. Wank, S. Perl, W. Cook, M. J. Olnes, K. D. Pradeep, J. C. Fuchs, M. Langweiler, E. Wang, J. P. McCoy, *PLoS One.* **2013**, *8(12)*, e76091.
[82] E. Codorean, A. Raducanu, L. Albulescu, C. Tanase, A. Meghea, R. Albulescu, *Roman. Biotechnol. Lett.* **2011**, *16(6)*, 6748–6759.
[83] T. K. Berthoud, M. N. Manaca, D. Quelhas, R. Aguilar, C. Guinovart, L. Puyol, A. Barbosa, P. L. Alonso, C. Dobaño, *Malar. J.* **2011**, *10*, 115.
[84] J. E. Sims, D. E. Smith, *Nat. Rev. Immunol.* **2010**, *10(2)*, 89–102.
[85] F. A. Bozza, J. I. Salluh, A. M. Japiassu, M. Soares, E. F. Assis, R. N. Gomes, M. T. Bozza, H. C. Castro-Faria-Neto, P. T. Bozza, *Crit Care.* **2007**, *11(2)*, R49.
[86] M. D. C. Cacemiro, J. G. Cominal, M. G. Berzoti-Coelho, R. Tognon, N. S. Nunes, B. Simões, Í. S. Pereira, D. Carlos, L. H. Faccioli, L. L. Figueiredo-Pontes, F. G. Frantz, F. A. Castro, *Sci. Rep.* **2020**, *10(1)*, 7032.
[87] C. Heijmans-Antonissen, F. Wesseldijk, R. J. Munnikes, F. J. Huygen, P. van der Meijden, W. C. Hop, H. Hooijkaas, F. J. Zijlstra, *Mediators Inflammation* **2006**, *2006(1)*, 28398.
[88] F. Berthier, C. Lambert, C. Genin, J. Bienvenu, *Clin. Chem. Lab. Med.* **1999**, *37(5)*, 593–599.
[89] R. P. Huang, *Methods Mol. Biol.* **2004**, *264*, 215–231.
[90] R. P. Huang, R. Huang, Y. Fan, Y. Lin, *Anal. Biochem.* **2001**, *294(1)*, 55–62.
[91] Y. Lin, R. Huang, N. Santanam, Y. G. Liu, S. Parthasarathy, R. P. Huang, *Cancer Lett.* **2002**, *187(1–2)*, 17–24.
[92] Y. Lin, R. Huang, X. Cao, S. M. Wang, Q. Shi, R. P. Huang, *Clin. Chem. Lab. Med.* **2003**, *41(2)*, 139–145.
[93] C. L. Ho, T. L. Lasho, J. H. Butterfield, A. Tefferi, *Leuk. Res.* **2007**, *31(10)*, 1389–1392.
[94] C. Schröder, A. Jacob, S. Tonac, T. P. Radon, M. Sill, M. Zucknick, S. Rüffer, E. Costello, J. P. Neoptolemos, T. Crnogorac-Jurcevic, A. Bauer, K. Fellenberg, J. D. Hoheisel, *Mol. Cell. Proteomics* **2010**, *9(6)*, 1271–1280.
[95] D. R. Thévenot, K. Toth, R. A. Durst, G. S. Wilson, *Biosens. Bioelectron.* **2001**, *16(1–2)*, 121–131.
[96] Y. H. Lee, R. Mutharasan, in *Sensor Technology Handbook, 1st ed.,* (Eds.: J. S. Wilson). *Newnes*, UK, **2005**. pp. 161–180.
[97] J. L. Hammond, N. Formisano, P. Estrela, S. Carrara, J. Tkac, *Electrochemical biosensors and nanobiosensors. Essays Biochem.* **2016**, *60(1)*, 69–80.
[98] C. M. Silveira, T. Monteiro, M. G. Almeida, *Biosensors* (Basel). **2016**, *6(4)*, 51.
[99] S. W. Loo, T. S. Pui, *Sensors* (Basel). **2020**, *20(7)*, 1854.
[100] L. Gonzalez-Macia, A. Morrin, M. R. Smyth, A. J. Killard, *Analyst.* **2010**, *135(5)*, 84–867.
[101] C. W. Foster, R. O. Kadara, C. E. Banks, in *Screen-Printing Electrochemical Architectures, 1st ed.*, *Springer*, *Cham* (Switzerland). **2016**, pp. 13–23.
[102] A. Albanese, P. S. Tang, W. C. Chan, *Annu. Rev. Biomed. Eng.* **2012**, *14*, 1–16.
[103] M. S. Verma, P. Z. Chen, L. Jones, F. X. Gu, *Sens Biosensing Res.* **2015**, *5*, 13–18.
[104] M. Pumera, A. Escarpa, *Electrophoresis.* **2009**, *30(19)*, 3315–3323.
[105] S. Campuzano, M. Pedrero, M. Gamella, V. Serafín, P. Yáñez-Sedeño, J. M. Pingarrón, *Sensors* (Basel). **2020**, *20(12)*, 3376.
[106] J. Orozco, S. Campuzano, D. Kagan, M. Zhou, W. Gao, J. Wang, *Anal. Chem.* **2011**, *83(20)*, 7962–7969.

[107] D. Vilela, J. Orozco, G. Cheng, S. Sattayasamitsathit, M. Galarnyk, C. Kan, J. Wang, A. Escarpa, *Lab Chip.* **2014**, *14(18)*, 3505–3509.
[108] D. Antuña-Jiménez, M. B. González-García, D. Hernández-Santos, P. Fanjul-Bolado, *Biosensors* (Basel). **2020**, *10(2)*, 9.
[109] L. Baptista–Pires, J. Orozco, P. Guardia, A. Merkoçi, *Small.* **2018**, *14(3)*, 1702746.
[110] C. Jiang, G. Wang, R. Hein, N. Liu, X. Luo, J. J. Davis, *Chem. Rev.* **2020**, *120(8)*, 3852–3889.
[111] E. Sardini, M. Serpelloni, S. Tonello, *Biosensors* (Basel). **2020**, *10(11)*, 166.
[112] C. Jiang, M. T. Alam, S. M. Silva, S. Taufik, S. Fan, J. J. Gooding, *ACS Sens.* **2016**, *1*, 1432–1438.
[113] M. Qi, Y. Zhang, C. Cao, M. Zhang, S. Liu, G. Liu, *Anal. Chem.* **2016**, *88(19)*, 9614–9621.
[114] H. Wei, S. Ni, C. Cao, G. Yang, G. Liu, *ACS Sens.* **2018**, *3(8)*, 1553–1561.
[115] P. Kongsuphol, H. H. Ng, J. P. Pursey, S. K. Arya, C. C. Wong, E. Stulz, M. K. Park, *Biosens. Bioelectron.* **2014**, *61*, 274–279.
[116] J. Min, M. Nothing, B. Coble, H. Zheng, J. Park, H. Im, G. F. Weber, C. M. Castro, F. K. Swirski, R. Weissleder, H. Lee, *ACS Nano.* **2018**, *12(4)*, 3378–3384.
[117] A. Makaraviciute, A. Ramanaviciene, *Biosens. Bioelectron.* **2013**, *50*, 460–4671.
[118] J. Orozco, C. Jiménez-Jorquera, C. Fernández-Sánchez, *Bioelectrochemistry.* **2009**, *75(2)*, 176–181.
[119] J. Orozco, C. Jiménez-Jorquera, C. Fernández-Sánchez, *Electroanalysis.* **2012**, *24*, 635–642.
[120] M. C. Brothers, D. Moore, M. S. Lawrence, J. Harris, R. M. Joseph, E. Ratcliff, O. N. Ruiz, N. Glavin, S. S. Kim, *Sensors* (Basel). **2020**, *20(8)*, 2246.
[121] D. Mandler, S. Kraus-Ophir, *J. Solid State Electrochem.* **2011**, *15*, 1535.
[122] N. G. Welch, J. A. Scoble, B. W. Muir, P. J. Pigram, *Biointerphases.* **2017**, *12(2)*, 02D301.
[123] J. Pinson, F. Podvorica, *Chem. Soc. Rev.* **2005**, *34(5)*, 429–439.
[124] B. P. Corgier, A. Laurent, P. Perriat, L. J. Blum, C. A. Marquette, *Angew. Chem. Int. Ed. Engl.* **2007**, *46(22)*, 4108–4110.
[125] A. K. Trilling, J. Beekwilder, J. H. Zuilhof, *Analyst.* **2013**, *138(6)*, 1619–1627.
[126] M. Shen, J. Rusling, C. K. Dixit, *Methods.* **2017**, *116*, 95–111.
[127] B. Johnsson, S. Löfås, G. Lindquist, A. Edström, R. M. Müller, A. Hansson, *J. Mol. Recognit.* **1995**, *8(1–2)*, 125–131.
[128] M. Kondzior, I. Grabowska, *Sensors* (Basel). **2020**, 20(7), 2014.
[129] K. Dave, N. Pachauri, A. Dinda, P. R. Solanki, *Appl. Surf. Sci.* **2019**, *463*, 587–595.
[130] N. Ruecha, K. Shin, O. Chailapakul, N. Rodthongkum, *Sens. Actuators B* **2019**, *279*, 298–304.
[131] E. Sánchez-Tirado, A. González-Cortés, P. Yáñez-Sedeño, J. M. Pingarrón, *Talanta.* **2020**, *211*, 120761.
[132] Y. Zhang, Y. Yan, B. Zhang, W. Zhu, Y. He, H. Huang, J. Li, Z. Jiang, S. Tan, X. Cai, *J. Solid-State Electron.* **2015**, *19*, 3111–3119.
[133] C. Russell, A. C. Ward, V. Vezza, P. Hoskisson, D. Alcorn, D. P. Steenson, D. K. Corrigan, *Biosens. Bioelectron.* **2019**, *126*, 806–814.
[134] Y. S. Kim, N. H. Raston, M. B. Gu, *Biosens. Bioelectron.* **2016**, *76*, 2–19.
[135] A. Hanif, R. Farooq, M. U. Rehman, R. Khan, S. Majid, M. A. Ganaie, *Saudi Pharm. J.* **2019**, *27(3)*, 312–319.
[136] L. S. Kumar, X. Wang, J. Hagen, R. Naik, I. Papautsky, J. Heikenfeld, *Anal. Methods* **2016**, *8*, 3440–3444.
[137] M. Tertis, P. I. Leva, D. Bogdan, M. Suciu, F. Graur, C. Cristea, *Biosens. Bioelectron.* **2019**, *137*, 123–132.
[138] Y. Liu, N. Tuleouva, E. Ramanculov, A. Revzin, *Anal. Chem.* **2010**, *82(19)*, 8131–8136.
[139] Y. Liu, Q. Zhou, A. Revzin, *Analyst.* **2013**, *138(15)*, 4321–4326.
[140] M. H. Ghalehno, M. Mirzaei, M. Torkzadeh-Mahani, *Mikrochim. Acta.* **2018**, *185(3)*, 165.
[141] P. Miao, D. Yang, X. Chen, Z. Guo, Y. Tang, *Microchim. Acta* **2017**, *184*, 3901–3907.
[142] C. Cao, F. Zhang, E. M. Goldys, F. Gao, G. Liu, *Trends Anal Chem.* **2018**, *102*, 379–396.
[143] P. Dauphin-Ducharme, K. Yang, N. Arroyo-Currás, K. L. Ploense, Y. Zhang, J. Gerson, M. Kurnik, T. E. Kippin, M. N. Stojanovic, K. W. Plaxco, *ACS Sens.* **2019**, *4(10)*, 2832–2837.
[144] N. Arroyo-Currás, G. Ortega, D. A. Copp, K. L. Ploense, Z. A. Plaxco, T. E. Kippin, J. P. Hespanha, K. W. Plaxco, *ACS Pharmacol Transl Sci.* **2018**, *1(2)*, 110–118.
[145] N. Arroyo-Currás, J. Somerson, P. A. Vieira, K. L. Ploense, T. E. Kippin, K. W. Plaxco, *Proc. Natl. Acad. Sci. USA* **2017**, *114(4)*, 645–650.
[146] P. Dauphin-Ducharme, K. W. Plaxco, *Anal. Chem.* **2016**, *88(23)*, 11654–11662.
[147] H. Li, P. Dauphin-Ducharme, G. Ortega, K. W. Plaxco, *J. Am. Chem. Soc.* **2017**, *139(32)*, 11207–11213.
[148] B. S. Ferguson, D. A. Hoggarth, D. Maliniak, K. Ploense, R. J. White, N. Woodwar, K. Hsieh, A. J. Bonham, M. Eisenstein, T. E. Kippin, K. W. Plaxco, H. T. Soh, *Sci. Transl. Med.* **2013**, *5(213)*, 213ra165.
[149] P. Chen, N. T. Huang, M. T. Chung, T. T. Cornell, K. Kurabayashi, *Adv. Drug Delivery Rev.* **2015**, *95*, 90–103.
[150] A. S. Tanak, S. Muthukumar, S. Krishnan, K. L. Schully, D. V. Clark, S. Prasad, *Biosens. Bioelectron.* **2021**, *171*, 112726.
[151] D. Sankhala, S. Muthukumar, S. Prasad, *SLAS Technol.* **2018**, *23(6)*, 529–539.
[152] A. S. Tanak, S. Muthukumar, I. A. Hashim, S. Prasad, *Sci. Rep.* **2020**, *10(1)*, 18804.
[153] N. B. Mincu, V. Lazar, D. Stan, C. M. Mihailescu, R. Iosub, A. L. Mateescu, *Diagnostics* (Basel). **2020**, *10(8)*, 517.
[154] C. Zhao, M. M. Thuo, X. Liu, *Sci. Technol. Adv. Mater.* **2013**, *14(5)*, 054402.
[155] G. M. Whitesides, *Nature.* **2006**, *442(7101)*, 368–373.
[156] A. Bange, H. B. Halsall, W. R. Heineman, *Biosens. Bioelectron.* **2005**, *20(12)*, 2488–2503.
[157] B. Wang, I. Jansson, J. B. Schenkman, J. F. Rusling, *Anal. Chem.* **2005**, *77(5)*, 1361–136.
[158] B. V. Chikkaveeraiah, A. Bhirde, R. Malhotra, V. Patel, J. S. Gutkind, J. F. Rusling, *Anal. Chem.* **2009**, *81(21)*, 9129–9134.
[159] B. V. Chikkaveeraiah, H. Liu, V. Mani, F. Papadimitrakopoulos, J. F. Rusling, *Electrochem. Commun.* **2009**, *11(4)*, 819–822.
[160] B. S. Munge, C. E. Krause, R. Malhotra, V. Patel, J. S. Gutkind, J. F. Rusling, *Electrochem. Commun.* **2009**, *11(5)*, 1009–1012.
[161] B. V. Chikkaveeraiah, V. Mani, V. Patel, J. S. Gutkind, J. F. Rusling, *Biosens. Bioelectron.* **2011**, *26(11)*, 4477–4483.
[162] B. A. Otieno, C. E. Krause, A. Latus, B. V. Chikkaveeraiah, R. C. Faria, J. F. Rusling, *Biosens. Bioelectron.* **2014**, *53*, 268–274.

[163] C. E. Krause, B. A. Otieno, G. W. Bishop, G. Phadke, L. Choquette, R. V. Lalla, D. E. Peterson, J. F. Rusling, *Anal. Bioanal. Chem.* **2015**, *407(23)*, 7239–7243.
[164] C. K. Tang, A. Vaze, J. F. Rusling, *Lab Chip.* **2012**, *12(2)*, 281–286.
[165] R. Malhotra, V. Patel, B. V. Chikkaveeraiah, B. S. Munge, S. C. Cheong, R. B. Zain, M. T. Abraham, D. K. Dey, J. S. Gutkind, J. F. Rusling, *Anal. Chem.* **2012**, *84(14)*, 6249–6255.
[166] C. K. Tang, A. Vaze, M. Shen, J. F. Rusling, *ACS Sens.* **2016**, *1(8)*, 1036–1043.
[167] G. Liu, C. Cao, S. Ni, S. Feng, H. Wei, *Microsyst Nanoeng.* **2019**, *5(35)*, 1–11.
[168] J. Yan, V. A. Pedrosa, A. L. Simonian, A. Revzin, *ACS Appl. Mater. Interfaces.* **2010**, *2(3)*, 748–755.
[169] Y. Liu, J. Yan, M. C. Howland, T. Kwa, A. Revzin, *Anal. Chem.* **2011**, *83(21)*, 8286–8292.
[170] T. Kwa, Q. Zhou, Y. Gao, A. Rahimian, L. Kwon, Y. Liu, A. Revzin, *Lab Chip.* **2014**, *14(10)*, 1695–1704.
[171] Y. Liu, Y. Liu, Z. Matharu, A. Rahimian, A. Revzin, *Biosens. Bioelectron.* **2015**, *64*, 43–50.
[172] Q. Zhou, D. Patel, T. Kwa, A. Haque, Z. Matharu, G. Stybayeva, Y. Gao, A. M. Diehl, A. Revzin, *Lab Chip.* **2015**, *15(23)*, 4467–4478.
[173] M. Morales, D. Pérez, L. Correa, L. Restrepo, *Toxicol. in Vitro.* **2016**, *36*, 89—96.
[174] N. Vasilakis, K. I. Papadimitriou, D. Evans, H. Morgan, T. Prodromakis, *HI–POCT, Cancun.* **2016**, 126–129.
[175] D. Moschou, L. Greathead, P. Pantelidis, P. Kelleher, H. Morgan, T. Prodromakis, *Biosens. Bioelectron.* **2016**, *86*, 805–810.
[176] D. Evans, K. I. Papadimitriou, N. Vasilakis, P. Pantelidis, P. Kelleher, H. Morgan, T. Prodromakis, *Sensors* (Basel). **2018**, *18(11)*, 4011.
[177] D. Evans, K. I. Papadimitriou, L. Greathead, N. Vasilakis, P. Pantelidis, P. Kelleher, H. Morgan, T. Prodromakis, *Sci. Rep.* **2017**, *7(1)*, 685.
[178] M. Gutiérrez-Capitán, A. Baldi, C. Fernández-Sánchez, *Sensors* (Basel). **2020**, *20(4)*, 967.
[179] V. N. Ataide, L. F. Mendes, L. I. Gama, W. R. de Araujo, T. R. Paixão, *Anal. Methods.* **2020**, *12*, 1030–1054.
[180] N. Nesakumar, S. Kesavan, C. Z. Li, S. Alwarappan, *J. Anal. Test.* **2019**, *3*, 3–18.
[181] Y. Xia, J. Si, Z. Li, *Biosens. Bioelectron.* **2016**, *77*, 774–789.
[182] C. Renault, K. Scida, K. N. Knust, S. E. Fosdick, R. M. Crooks, *J Electrochem Sci Te.* **2013**, *4(4)*, 146–152.
[183] F. Volpetti, J. Garcia-Cordero, S. J. Maerkl, *PLoS One.* **2015**, *10(2)*, e0117744.
[184] J. Cao, J. Seegmiller, N. Q. Hanson, C. Zaun, D. Li, *Clin. Proteomics.* **2015**, *12*, 28.
[185] P. Aldo, G. Marusov, D. Svancara, J. David, G. Mor, *Am. J. Reprod. Immunol. (1980-1984)* **2016**, *75(6)*, 678–693.
[186] H. E. Lynch, A. M. Sanchez, M. P. D'Souza, W. Rountree, T. N. Denny, M. Kalos, G. D. Sempowski, *J. Immunol. Methods.* **2014**, *409*, 62–71.
[187] X. Zhou, M. S. Fragala, J. E. McElhaney, G. A. Kuchel, *Curr. Opin. Clin. Nutr. Metab. Care.* **2010**, *13(5)*, 541–547.
[188] S. S. Khan, M. S. Smith, D. Reda, A. F. Suffredini, J. P. Jr McCoy, *Cytometry Part B* **2004**, *61(1)*, 35–39.
[189] G. Li, M. Qi, M. R. Hutchinson, G. Yang, E. M. Goldys, *Biosens. Bioelectron.* **2016**, *79*, 810–821.
[190] R. N. Monastero, S. Pentyala, *Int J Inflam.* **2017**, *2017*, 4309485.
[191] W. J. Wiersinga, A. Rhodes, A. C. Cheng, S. J. Peacock, H. C. Prescott, *Jama.* **2020**, *324(8)*, 782–793.
[192] V. Mani, B. V. Chikkaveeraiah, V. Pate, J. S. Gutkind, J. F. Rusling, *ACS Nano.* **2009**, *3(3)*, 585–594.
[193] C. T. Lin, S. M. Wang, *Front. Biosci.* **2005**, *10*, 99106.
[194] J. H. Luong, K. B. Male, J. D. Glennon, *Biotechnol. Adv.* **2008**, *26(5)*, 492–500.
[195] K. Mahato, P. K. Maurya, P. Chandra, *3 Biotech.* **2018**, *8(3)*, 149.

Received: May 4, 2021
Accepted: June 19, 2021
Published online on ■■, ■■

REVIEW

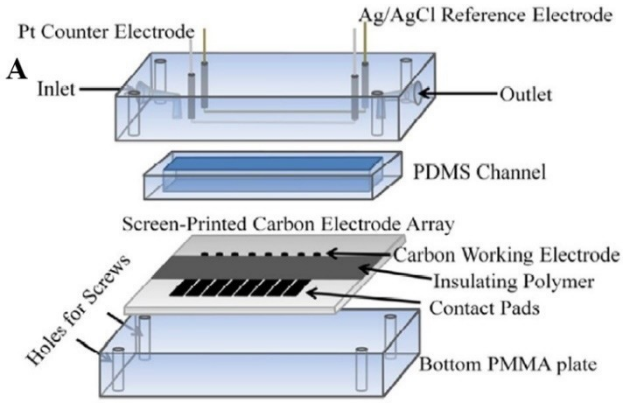

*D. J. Pérez, E. B. Patiño, J. Orozco**